



HAL
open science

A bacterial protein targets the BAHD1 chromatin complex to stimulate type III interferon response

Alice Lebreton, Goran Lakisic, Viviana Job, Lauriane Fritsch, To Nam Tham, Ana Camejo, Pierre-Jean Matteï, Béatrice Regnault, Marie-Anne Nahori, Didier Cabanes, et al.

► To cite this version:

Alice Lebreton, Goran Lakisic, Viviana Job, Lauriane Fritsch, To Nam Tham, et al.. A bacterial protein targets the BAHD1 chromatin complex to stimulate type III interferon response. *Science*, 2011, 331 (6022), pp.1319-21. 10.1126/science.1200120 . cea-00819299

HAL Id: cea-00819299

<https://cea.hal.science/cea-00819299>

Submitted on 26 Jul 2020

HAL is a multi-disciplinary open access archive for the deposit and dissemination of scientific research documents, whether they are published or not. The documents may come from teaching and research institutions in France or abroad, or from public or private research centers.

L'archive ouverte pluridisciplinaire **HAL**, est destinée au dépôt et à la diffusion de documents scientifiques de niveau recherche, publiés ou non, émanant des établissements d'enseignement et de recherche français ou étrangers, des laboratoires publics ou privés.

A Bacterial Protein Targets the BAHD1 Chromatin Complex to Stimulate Type III Interferon Response

Alice Lebreton^{1,2,3}, Goran Lakisic⁴, Viviana Job⁵, Lauriane Fritsch⁶, To Nam Tham^{1,2,3}, Ana Camejo⁷, Pierre-Jean Matteï⁵, Béatrice Regnault⁸, Marie-Anne Nahori^{1,2,3}, Didier Cabanes⁷, Alexis Gautreau⁴, Slimane Ait-Si-Ali⁶, Andréa Dessens⁵, Pascale Cossart^{1,2,3*} and H el ene Bierne^{1,2,3*}

1. Institut Pasteur, Unit e des Interactions Bact eries Cellules, Paris, F-75015 France;
 2. Inserm, U604, Paris, F-75015 France;
 3. INRA, USC2020, Paris, F-75015 France.
 4. CNRS UPR3082, Laboratoire d'Enzymologie et de Biochimie Structurales, Gif-sur-Yvette, F-91198 France.
 5. Institut de Biologie Structurale, Bacterial Pathogenesis Group, UMR 5075 (CNRS/CEA/UJF), Grenoble, France.
 6. CNRS UMR7216, Universit e Paris 7 Diderot, Paris, F-75013 France.
 7. Institute for Molecular and Cell Biology, Porto, Portugal.
 8. Institut Pasteur, G enopole, Paris, F-75015 France.
- * To whom correspondence should be addressed. helene.bierne@inrae.fr; pascale.cossart@pasteur.fr

This is a post-print version of an article published by the American Association for the Advancement of Science in *Science* in March 2011, available online as [doi:10.1126/science.1200120](https://doi.org/10.1126/science.1200120)

One-sentence summary

A virulence factor secreted by *Listeria monocytogenes* alleviates BAHD1-mediated silencing of interferon- λ stimulated genes.

Abstract

Intracellular pathogens such as *Listeria monocytogenes* subvert cellular functions through the interaction of bacterial effectors with host components. Here we found that a secreted listerial virulence factor, LntA, could target the chromatin repressor BAHD1 in the host cell nucleus to activate IFN-stimulated genes (ISGs). IFN- λ expression was induced in response to infection of epithelial cells with bacteria lacking LntA; however, the BAHD1-chromatin associated complex repressed downstream ISGs. In contrast, in cells infected with *lntA*-expressing bacteria, LntA prevented BAHD1 recruitment to ISGs and stimulated their expression. Murine listeriosis decreased in *BAHD1*^{+/-} mice or when *lntA* was constitutively expressed. Thus the LntA-BAHD1 interplay may modulate IFN- λ -mediated immune response to control bacterial colonization of the host.

Listeria monocytogenes is a food-borne pathogen that can cause serious illness in pregnant women and immunocompromised individuals (1). This intracellular bacterium uses an arsenal of effectors to exploit cellular functions in various ways (2). Host cells respond to this invasion by turning on appropriate defense transcriptional programs (3). *Listeria* and other pathogens can manipulate chromatin to reprogram host transcription (4, 5). However, very few bacterial molecules have been shown to enter eukaryotic cell nuclei, and knowledge about microbial factors that may act directly on the chromatin-regulatory machinery is limited (6).

To identify factors involved in bacterial pathogenicity, we screened the *L. monocytogenes* strain EGDe genome for genes encoding secreted proteins absent in non-pathogenic *Listeria* species. *lmo0438/lntA* (*listeria nuclear targeted protein A*) was one such gene (fig. S1A). *lntA* was expressed at very low levels by the EGDe strain grown in brain-heart infusion (BHI) medium (fig. S1B, 7). Two major regulators of virulence genes, PrfA and σ_B , were required for basal *lntA* transcription (fig. 1A). *lntA* expression was significantly higher in bacteria harvested from spleens of infected mice 48 h after intravenous inoculation, compared to bacteria grown in BHI (fig. 1B). In addition, deletion of *lntA* led to a decrease in bacterial colonization of spleens and livers, as well as blood bacteraemia (fig. 1B). *lntA* thus contributes to *L. monocytogenes* virulence. It encodes a 205-amino acid basic protein with a N-terminal signal peptide but no sequence similarity with any known polypeptide. The 2.3 Å resolution structure of LntA reveals a compact α -helical fold (fig. S2, PDB ID#2xl4). Consistent with low *lntA* transcription levels in vitro, LntA was undetectable in either total extracts or supernatants of wild type (WT) bacteria grown in BHI (fig. 1C).

To address the role of LntA during *L. monocytogenes* cellular infection, we generated strains that constitutively expressed *lntA* under the control of a heterologous promoter, either on the chromosome (*lntA_{c+}*) or on a plasmid in fusion with the V5 tag (*lntA_{V5+}*) (tables S1, S2). Both strains produced and secreted LntA (fig. 1C and S1C), and showed no noticeable difference in entry or multiplication in cultured cells compared to the WT or *lntA*-deficient strains (Δ *lntA*, *lntA₋* or *lntA_{c-}*) (table S3A, fig. S3). Secreted LntA accumulated in the nucleus of fibroblasts after 22 h of infection with *lntA_{V5+}* bacteria (fig. 1D and S4A). We thus assessed whether LntA interacted with nuclear proteins in a large-scale yeast two-hybrid screen of a human cDNA library. One of the strongest LntA interactors was BAHD1, a silencing factor that orchestrates heterochromatin assembly at specific genes such as *IGF2* (8). A fusion of LntA with glutathione-S-transferase (GST) pulled down V5-tagged BAHD1 from nuclear extracts, confirming the capacity of LntA to specifically interact with BAHD1 (fig. 1E). When produced ectopically in human fibroblasts, LntA co-localized with BAHD1-YFP-induced heterochromatin nuclear foci (8), both in fixed (LntA-V5, fig. 1F) and in living cells (LntA-CFP, fig. S4B).

Because BAHD1 is involved in gene silencing, LntA might control host gene expression. To assess this hypothesis, we performed a transcriptome analysis of LoVo epithelial cells infected for 24 h either with *lntA_{V5+}* or *lntA₋* bacteria (GEO database, GSE26414). The *lntA_{V5+}* bacteria specifically up-regulated the expression of a subset of genes, out of which 39 displayed more than a 2-fold induction (table S4). 83% of these genes belonged to the interferon-inducible genes regulon: 28 are known ISGs, including 3 genes (*IL29*, *IL28A* and *IL28B*) that encode type III interferons (IFN- λ 1, - λ 2 and - λ 3), and 4 are predicted ISGs. LntA may thus play a role in the IFN-III-mediated immune response. This pathway controls various viral infections, especially in epithelial tissues (9-13).

We confirmed that WT *L. monocytogenes* triggered the expression of IFN- λ 2 in intestinal LoVo and placental JEG-3 epithelial cells (fig. 2A; fig. S5A); type I IFN- β 1 was also induced, but type II IFN- γ was undetectable. However, the induction of downstream ISGs was modest

(fig. 2A), except for *CCL5*, which, like *IFN- λ* genes, is controlled both by NF- κ B and IRFs (fig. S9, 14). These data suggested that interferon signaling was down-regulated in infected cells. We wondered whether the host factor BAHD1 could act as a repressor of ISGs, as it does for *IGF2* (fig. S4B, 8). Knockdown of *BAHD1* had no or minor effect on ISG expression in non-infected LoVo cells (fig. 2B). However, infection of these BAHD1-depleted cells with *L. monocytogenes* induced the expression of several ISGs, highlighting that BAHD1 could act as a negative regulator of this pathway upon bacterial-triggered signaling (fig. 2B, S5B).

ISG expression is governed by IRF/STAT transcriptional activators and by chromatin structure regulators. Except for HP1 proteins, found as BAHD1 partners (8) and repressing ISGs (15), there is no reported link between BAHD1 and STAT signaling. To address whether BAHD1 was associated with other proteins involved in ISG regulation, we purified the BAHD1-associated complex from the chromatin fraction of HEK293 cells expressing His6-Protein C-tagged BAHD1 (HPT-BAHD1) by tandem affinity chromatography (fig. 2C, S6). Mass spectrometry analysis of the complex revealed several polypeptides involved in chromatin and transcriptional regulation, including KAP1, HP1 γ and histone deacetylases HDAC1/2, as confirmed by immunoblots (fig. 2C). HDAC1/2 directly binds STAT (16), as does the scaffolding protein KAP1, which represses both basal and IFN-I-mediated STAT-driven transcription (17, 18). We investigated whether KAP1 also repressed ISGs during infection with *Listeria*. *KAP1* knockdown induced ISG expression in non-infected cells, and bacterial infection greatly enhanced this induction (fig. 2B, S5C). The BAHD1/KAP1-corepressor complex thus inhibits ISGs downstream of IFN-III stimulation during *L. monocytogenes* infection.

Because WT *L. monocytogenes* does not express *lntA* in vitro, we further explored the role played by LntA in the IFN-III signaling pathway using *lntA*-constitutive strains. In agreement with the transcriptome data (table S4), ISG expression was higher in LoVo cells infected with *lntA*^{V5+} (fig. 3A) or *lntA*^{c+} (fig. S5D) bacteria, compared to non-infected cells or *lntA*-infected cells. This effect was observed only in epithelial cell lines (fig. S5E). The expression of *CCL5* (fig. 3A) and *IFN- λ 2* (fig. S5F), which are ISGs themselves, was also increased upon infection with *lntA*-constitutive strains. Thus, LntA can activate ISGs specifically in *Listeria*-infected epithelial cells, phenocopying BAHD1 depletion (fig. 2B, S5B). As LntA interacted with BAHD1, we addressed whether it inhibited BAHD1-mediated silencing. Chromatin immunoprecipitation (ChIP) revealed that the recruitment of BAHD1 at the promoter of representative ISGs (*IFIT3* and *IFITM1*) was impaired in *lntA*^{V5+}-infected cells, compared to *lntA*-infected cells (fig. 3B). This correlated with an enrichment of acetyl-H3K9 at these genes, consistent with increased transcriptional activity (fig. 3A). Thus, by displacing the BAHD1/HDAC complex from ISGs, LntA de-represses these genes in infected cells (fig. S7).

Neither *lntA* expression (fig. S3, table S3), nor cellular stimulation with recombinant IFN- λ 2 (fig. S8), altered bacterial infection in tissue-cultured LoVo cells. We thus assessed the consequences of LntA/BAHD1 interactions on the outcome of infection in vivo. To this end, (i) we infected BALB/c mice with *lntA*-constitutive or *lntA*-deficient bacteria and (ii) we generated C57BL/6 *BAHD1*^{+/-} mice (fig. S9, S10) and infected them with WT bacteria. We observed a strong decrease in bacterial burden in spleens and livers of BALB/c mice infected with *lntA*^{c+} or *lntA*^{V5+} relative to Δ *lntA* or WT bacteria, while the IFN- λ 3 concentration increased in infected organs (fig. 3C and S11). Thus, constitutive expression of *lntA* promotes the IFN-III response and decreases bacterial colonization in vivo. Moreover, in *BAHD1*^{+/-} mice infected with WT *L. monocytogenes*, the bacterial burden in organs was reduced compared to *BAHD1*^{+/+} mice (fig. 3D). Thus increasing *lntA* expression in *Listeria* had similar effects as impairing *BAHD1* expression in the host, *i.e.* decreasing infection. Furthermore, while controlled secretion of LntA by WT bacteria is beneficial to the pathogen, either its constitutive

secretion or its absence is detrimental. We propose that a tight control of *lntA* expression during infection allows *Listeria* to fine-tune localized immune responses and escape antibacterial response (19). Given the tropism of *Listeria* (20) and IFN-III (9-13) for epithelia, unraveling the role of LntA in these tissues is now a key issue. Our work identifies the BAHDI complex as a negative regulator of ISGs in the context of listeriosis, and highlights the importance of chromatin remodeling in bacterial infections.

References

1. O. Dussurget, *Int Rev Cell Mol Biol* **270**, 1 (2008).
2. P. Cossart, A. Toledo-Arana, *Microbes Infect* **10**, 1041 (Jul, 2008).
3. S. C. Corr, L. A. O'Neill, *Cell Microbiol*, (Feb 2, 2009).
4. M. A. Hamon, P. Cossart, *Cell Host Microbe* **4**, 100 (Aug 14, 2008).
5. K. Paschos, M. J. Allday, *Trends Microbiol* **18**, 439 (Oct, 2010).
6. A. P. Bhavsar, J. A. Guttman, B. B. Finlay, *Nature* **449**, 827 (Oct 18, 2007).
7. Methods are available as supporting material on Science Online.
8. H. Bierne *et al.*, *Proc Natl Acad Sci U S A* **106**, 13826 (Aug 18, 2009).
9. M. Li, X. Liu, Y. Zhou, S. B. Su, *J Leukoc Biol* **86**, 23 (Jul, 2009).
10. R. P. Donnelly, S. V. Kotenko, *J Interferon Cytokine Res* **30**, 555 (Aug, 2010).
11. M. Mordstein, T. Michiels, P. Staeheli, *J Interferon Cytokine Res* **30**, 579 (Aug, 2010).
12. G. Gallagher *et al.*, *J Interferon Cytokine Res* **30**, 603 (Aug, 2010).
13. J. E. Pulverer *et al.*, *J Virol* **84**, 8626 (Sep, 2010).
14. A. Casola *et al.*, *J Virol* **75**, 6428 (Jul 1, 2001).
15. M. Lavigne *et al.*, *PLoS Genet* **5**, e1000769 (Dec, 2009).
16. I. Nusinzon, C. M. Horvath, *Proc Natl Acad Sci U S A* **100**, 14742 (Dec 9, 2003).
17. S. Kamitani *et al.*, *Biochem Biophys Res Commun* **370**, 366 (May 30, 2008).
18. R. Tsuruma *et al.*, *Oncogene* **27**, 3054 (May 8, 2008).
19. Supporting discussion is available on Science Online.
20. M. Lecuit, *Clin Microbiol Infect* **11**, 430 (Jun, 2005).
21. We thank E. Gouin for anti-LntA antibodies; J-Y. Coppee for microarrays facilities at the IP Genopole; S. Jacquot and M.C. Birling at the Targeted Mutagenesis and Transgenesis department of the Mouse Clinical Institute (MCI/ICS), where was generated the *BAHDI*^{+/-} mouse line. Work in the Cossart laboratory received financial support from the Pasteur Institute, INRA, INSERM, ANR-ERANET-PathoGenomics (grant SPATELIS), French Ligue Nationale Contre le Cancer (LNCC RS10/75-76 Bierne) and ERC (Advanced Grant 233348). P-J.M. received a PhD fellowship from Région Rhône Alpes. Work in the Cabanes laboratory was supported by FCT (PTDC-SAU/MII/65406/2006; PhD fellowship to A.C. SFRH/BD/29314/2006) and ERANET-PathoGenomics (grant SPATELIS). P.C. is an international research scholar of the Howard Hughes Medical Institute.

Figures

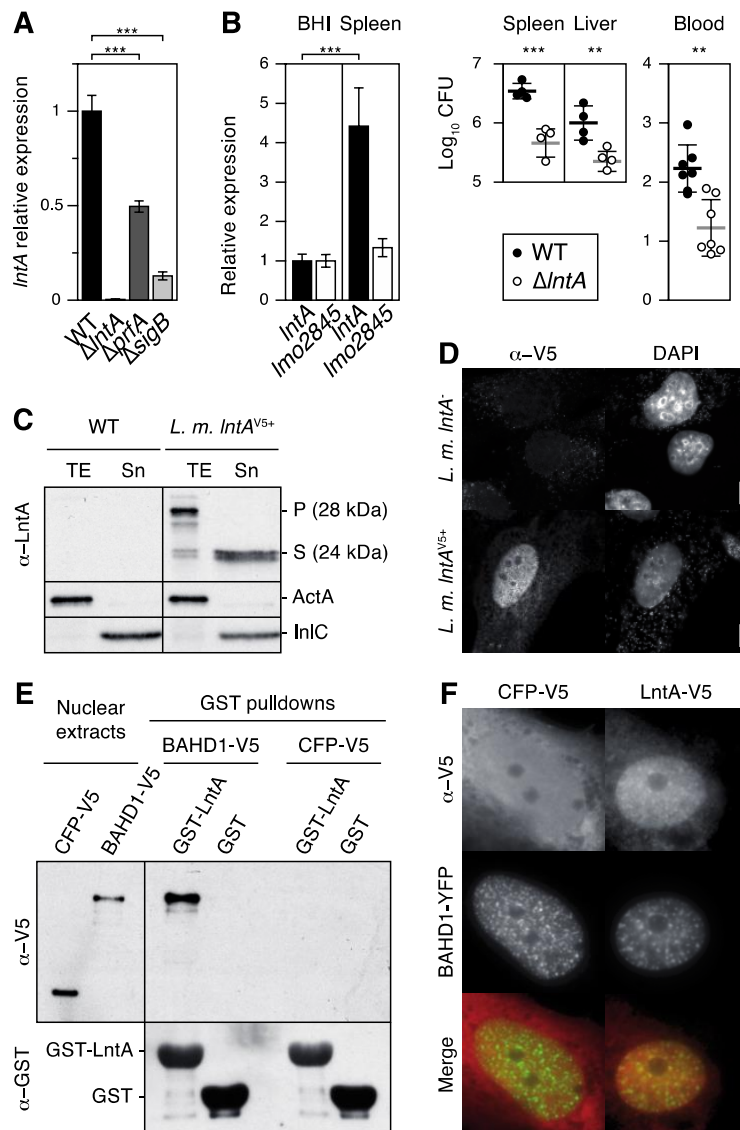


Fig. 1. The secreted virulence factor LntA targets the nuclear protein BAHD1. (A) *lntA* is regulated by PrfA and σ_B . qRT-PCR analysis of *lntA* levels in WT, $\Delta lntA$, $\Delta prfA$ or $\Delta sigB$ strains. (B) *lntA* is up-regulated and contributes to virulence 48 h post-infection in an intravenous mouse model. *Left*, qRT-PCR analysis of *lntA* and control *lmo2845* levels in WT *Listeria* extracted from spleens. *Right*, bacteria were numerated in organ or mL blood from mice infected with WT or $\Delta lntA$ strains. (A-B) **, $p < 0.01$; ***, $p < 0.001$ (two-tailed T-tests). (C) LntA is a secreted protein. Bacterial total extracts (TE) and supernatants (Sn) of WT or *lntA*^{v5+} strains were analyzed by immunoblot, with ActA and InlC used as controls. WT bacteria do not produce LntA in BHI. P, precursor; S, secreted. (D) LntA localizes to the nucleus of C3SV40 fibroblasts. V5 immunolabelling and DAPI staining in cells infected for 22 h with *lntA*- or *lntA*^{v5+} bacteria. (E) Purified LntA binds BAHD1. GST or GST-LntA were incubated with nuclear extracts from CFP-V5 or BAHD1-V5 –expressing HEK293 cells. Immunoblots of inputs and eluted fractions were probed with α -V5 or α -GST antibodies. (F) LntA localizes to BAHD1-induced heterochromatin foci. BAHD1-YFP and either LntA-V5 or CFP-V5 were co-transfected into C3SV40 cells and detected by immunofluorescence. (D, F) Bars, 5 μ m.

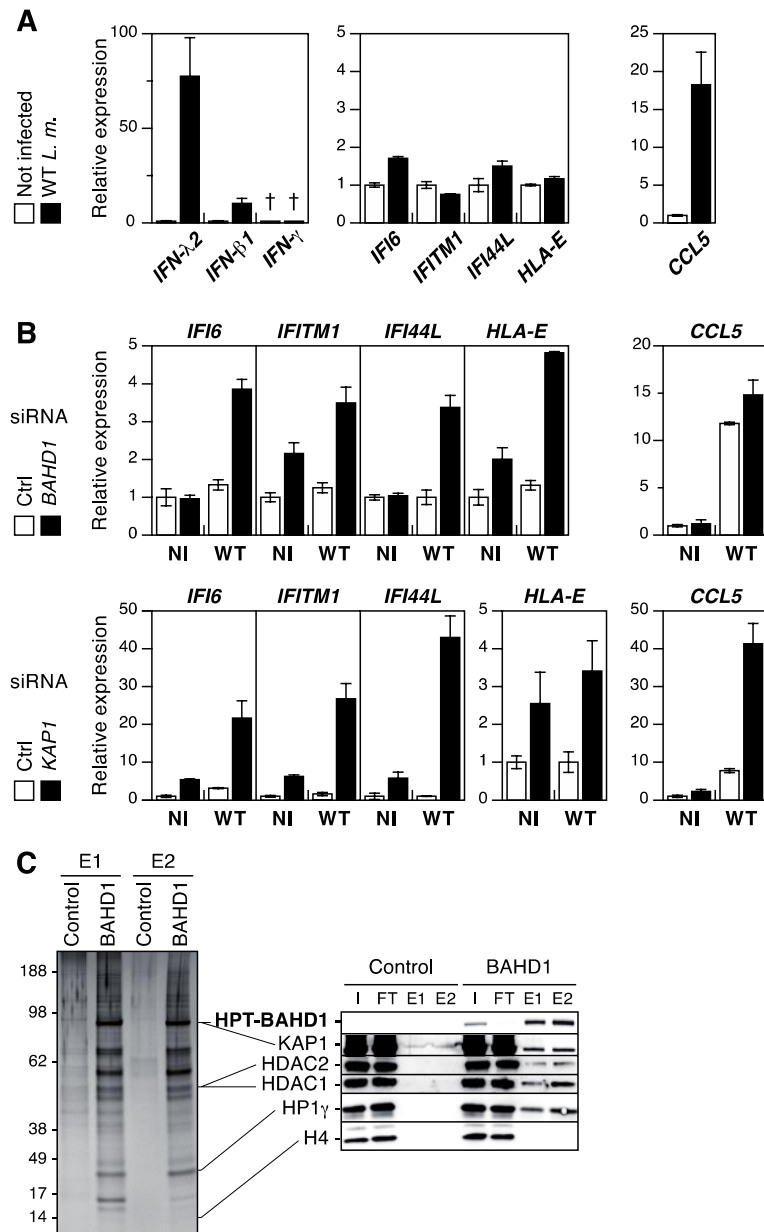


Fig. 2. The BAHD1 complex represses ISGs in *Listeria*-infected epithelial cells. (A) qRT-PCR analysis of *IFN* and *ISG* expression in response to *Listeria* infection in LoVo cells infected for 16 h with WT *L. monocytogenes*, compared to non-infected cells. *Left*: type I (*IFN-β1*), II (*IFN-γ*) and III (*IFN-λ2*) interferon genes. *Right*, various *ISGs*. †, below detection limits. (B) Quantification of *ISGs* mRNA in LoVo cells treated for 72 h with control siRNA, siRNA against *BAHD1* or *KAP1* and infected for 16 h (WT) or not (NI). (C) Tandem-affinity purification of the BAHD1-associated complex. Solubilized chromatin extracts from HEK293 cells expressing the HPT-BAHD1 fusion or control cells were first purified on anti-protein C affinity matrix, followed by polishing on nickel-sepharose. Eluted fractions from the first (E1) and second (E2) affinity columns were analyzed by colloidal coomassie staining (*left*) or immunoblot (*right*). I, input; FT, flow through from first column. Histone H4 was a control for non-specific binding of chromatin components.

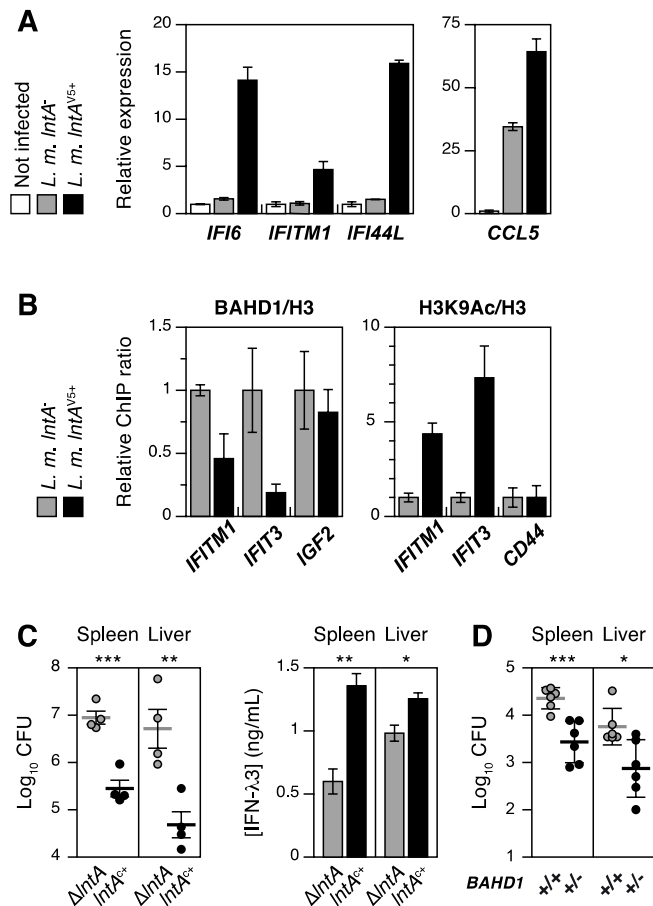


Fig. 3. LntA impairs BAHD1-mediated repression of ISGs. (A) LntA induces ISGs. mRNA levels were estimated by qRT-PCR on total RNA from LoVo cells infected for 16 h with *lntA*- or *lntA^{Δ5+}*, compared to non-infected cells. (B) LntA impairs BAHD1 recruitment and increases acetyl-H3 levels at ISGs. ChIP analysis was performed on LoVo cells infected as in (A), with antibodies against BAHD1 or H3K9Ac. Promoter DNA levels were assessed by qRT-PCR and normalized to cognate levels in histone H3-ChIP. (C) Constitutive expression of *lntA* in *Listeria* decreases bacterial burden during murine systemic listeriosis and triggers overproduction of IFN-III. Mice were infected intravenously with either Δ *lntA* or *lntA^{c+}* strains. *Left*, Colony forming units (CFU) per organ were numerated at 72 h post-infection. *Right*, Mouse IFN-λ3 concentration was quantified by ELISA in clarified total extracts of infected spleens and livers. (D) *BAHD1*^{+/-} mice are less sensitive to systemic listeriosis. *BAHD1*^{+/+} or isogenic *BAHD1*^{+/-} mice were infected intravenously with *L. monocytogenes* EGDe. Colony forming units (CFU) per organ were numerated at 72 h post-infection. (C-D) *, p < 0.05; **, p < 0.01; ***, p < 0.001.

Supporting online material

Material and Methods

Bacterial strains, culture conditions, plasmids and oligonucleotides
Human cell lines
Generation of *BAHD1*^{+/-} mice
Antibodies
Yeast two-hybrid (Y2H) screening
Transient transfections with plasmids or oligofection with siRNA duplexes
Cellular infections, entry and intracellular multiplication assays
Animal infections
Immunofluorescence analysis, live-cell imaging and image processing
Bacterial extracts, SDS-PAGE and immunoblots
GST-pulldowns
Expression and purification of LntA for cristallography
Crystallization, structure solution and refinement
Tandem affinity purification of the HPT-BAHD1-associated complex and mass spectrometry analysis
NanoLC-MS/MS analyses for protein identification
Sandwich ELISA measurement of mouse IFN- λ 3 in organ homogenates
Bacterial RNA extraction and qRT-PCR
Transcriptome analysis of infected cells
Human and mice RNA extraction and qRT-PCR
Chromatin immunoprecipitation experiments and site-specific PCR analysis

SOM text

Roles of type I, II and III interferons in listeriosis
Influence of the genetic background on the outcome of murine listeriosis

Supporting Figures

Fig. S1. Identification of *lntA* as a candidate virulence gene encoding a secreted protein.
Fig. S2. LntA folds into a compact helical structure.
Fig. S3. Deletion or constitutive expression of *lntA* does not alter bacterial invasion of host cells.
Fig. S4. LntA colocalizes with BAHD1 in the nucleus of human living cells.
Fig. S5. Expression of interferon genes and ISGs in response to *Listeria* infection.
Fig. S6. Tandem-affinity purification of the HPT-BAHD1 associated complex.
Fig. S7. Proposed model for BAHD1/LntA-mediated regulation of ISGs.
Fig. S8. Bacterial intracellular multiplication in LoVo cells is not altered by IFN- λ -stimulation.
Fig. S9. Verification of the *BAHD1* KO allele.
Fig. S10. Genotyping of *BAHD1*^{+/-} mice.
Fig. S11. Both deletion and constitutive expression of *lntA* in *Listeria* decrease bacterial burden during murine systemic listeriosis.

Supporting Tables

Table S1. Bacterial strains.
Table S2. Plasmids.
Table S3. Bacterial entry in LoVo cells is independent of *lntA* expression and is not altered by IFN- λ 2 treatment.
Table S4. Transcriptome data – genes activated by LntA in infected LoVo cells.
Table S5. Oligonucleotides.
Table S6. PCR products and digests for the validation of *BAHD1*^{+/-} mice.
Table S7. Crystallography. Data collection, phasing and refinement statistics.

References

Material and Methods

Bacterial strains, culture conditions, plasmids and oligonucleotides

Strains, plasmids and oligonucleotides used in this work are recapitulated in tables S1, S2, and S5, respectively. *Listeria* and *Escherichia coli* strains were grown in brain-heart infusion (BHI) or Luria-Bertani (LB) media (Difco), respectively, at 37°C. When appropriate, antibiotics were included in media at the following concentrations: kanamycin, 30 µg/ml; ampicillin, 100 µg/ml, colistin, 10 µg/ml; nalidixic acid, 50 µg/ml; erythromycin, 5 µg/ml; chloramphenicol, 7 µg/ml for *Listeria*, 35 µg/ml for *E. coli*.

For heterologous expression constructs of C-terminally tagged LntA fusions, the *lntA* (lmo0438, Gen-bank/EMBL accession number AL591975, 1) Open Reading Frame (ORF) without the sequence encoding the signal peptide (residues Gly₃₄ to Lys₂₀₅) was introduced into pcDNA3.1/V5-His-TOPO using the directional topoisomerase cloning system (Invitrogen). Fluorescence microscopy, two-hybrid and GST-fusion protein expression constructs were generated by sub-cloning *lntA* into pE-mCFP-N1 (2), pB27 (Hybrigenics) pET41a (Novagen), and pGEX-4T-1 (GE Healthcare) respectively.

To constitutively express *lntA* in *Listeria*, we inserted the complete *lntA* ORF, fused with a V5 tag, into the pP1 multicopy plasmid, downstream of the constitutive *P_{PRT}* promoter of the protease gene from *Streptococcus cremoris* (3). This plasmid expressing *lntA*-V5 was electroporated into *L. monocytogenes* EGDe, generating BUG2384 (referred to as *lntA*_{V5+}). As a control, the empty pP1 vector was electroporated into EGDe Δ *lntA*, generating BUG2466 (referred to as *lntA*₋).

We additionally designed a *Listeria* strain where a non-tagged copy of *lntA* was integrated in the *Listeria* genome at the *tRNA_{ARG}* locus using the pPL2 shuttle system (4). A pPL2 vector carrying a *PHYPER*-5'-*UTR_{hy}*-*lntA* transcriptional fusion was transformed into the EGDe Δ *lntA* strain by conjugation, yielding to the complemented strain BUG2822 (referred to as *lntA*_{c+}). A isogenic Δ *lntA*:pPL2 control strain was also generated with the empty pPL2 vector (BUG2820, referred to as *lntA*_{c-}). Selected integrants were confirmed by PCR.

To engineer a stable cell line producing the HPT-BAHD1 fusion, and a control cell line, we designed the following plasmids. First, the Tet operator sequence (TO) was introduced into pcDNA5/FRT-HPT-blue (a derivative of pcDNA5/FRT/V5-His from Invitrogen, 5). This gave rise to pcDNA5/FRT/TO-HPT-blue, allowing the N-terminal fusion of any inserted sequence with the HPT tag, e.g. a 6xHis tag, followed by the Protein C epitope and by a TEV cleavage site: MHHHHHH-EDQVDPRLIDGK-gggdydiptt-ENLYFQG-amgrp. Due to the Tet operator, the expression of the fusion is repressed by the Tet repressor in Flp-In T-Rex 293 cells (Invitrogen), but can be activated by addition of tetracycline to the culture medium. *BAHD1* was cloned in pcDNA5/FRT/TO-HPT-blue to give rise to pcDNA5/FRT/TO-HPT-*BAHD1*, expressing HPT-tagged *BAHD1* in a tetracycline-dependent manner. In the control pcDNA5/FRT/TO-HPT-blue plasmid, the tag is fused to a single T codon before the stop codon.

All constructs were verified by double-strand sequencing. Additional cloning details are available upon request.

Human cell lines

We used C3SV40 fibroblasts (6), intestinal epithelial LoVo cells (ATCC CCL-229), placental JEG-3 cells (ATCC HTB-36), U-937 and THP-1 monocytes (CRL-1593.2 and TIB-202 respectively), HEK293 embryonic kidney cells (CRL-1573), and HEK293-derived Flp-In T-Rex 293 cells (Invitrogen). C3SV40 cells were grown in RPMI 1640 (Gibco) supplemented with 10% FCS (Gibco); other cell lines were grown following ATCC or Invitrogen

recommendations. All cells were cultured at 37°C in a humidified atmosphere containing 10% CO₂.

Stable HEK293-HPT-BAHD1 and control HEK293-HPT-blue cells were generated as follows. Flp-In T-Rex 293 were transfected with the pcDNA5/FRT/TO-HPT-*BAHD1* or -blue plasmids, together with the plasmid encoding the Flp recombinase. Stable pool of transfectants having undergone integration of HPT-expressing plasmids at the single FRT locus were selected as described (7), with the exception that 15 µg/ml of Blasticidin (Invivogen) was added to the culture media in order to select for the maintenance of Tet repressor expression.

For BAHD1 complex purification, HEK293-HPT-BAHD1 and control -blue cells were grown in 3-L spinners in DMEM, 10% fetal calf serum, 1% Penicillin/Streptomycin under 5% CO₂ atmosphere. To induce the production of the HPT-BAHD1 fusion, tetracycline was added to cell culture media 24 h before cell recovery at a final concentration of 11 µg/ml. Cell pellets were recovered by centrifugation, PBS-washed, flash-frozen in liquid nitrogen and stored at -80°C until they were use for tandem affinity purification.

Generation of *BAHD1*^{+/-} mice

The *BAHD1* mutant mouse line was established at the MCI/ICS (Mouse Clinical Institute, Institut Clinique de la Souris, Illkirch, France; <http://www-mci.u-strasbg.fr>). The entire coding region of the *BAHD1* allele (Ensembl Gene ID: ENSMUSG00000040007) including the intronic sequences was replaced with a floxed neomycin cassette. The targeting vector was constructed as follows. A 4.3-kb fragment upstream of *BAHD1* exon 2 and a 4.3kb fragment downstream of *BAHD1* exon 7 were PCR-amplified and subcloned upstream and downstream of a floxed Neomycin (Neo) resistance cassette into an MCI proprietary vector, which contains the thymidine kinase gene for a negative selection. The linearized construct was electroporated in C57BL/6 mouse embryonic stem (ES) cells. After selection, targeted clones were identified by PCR amplification using external primers (Ef1/Nr1), and were further confirmed by Southern blot with an internal Neo probe and an external probe (table S6 and fig. S9). Five clones amongst 372 clones were positive. Two positive ES clones were injected into BALB/c recipient blastocysts and the derived male chimaeras showed efficient germline transmission. C57BL/6 mice derived from clone #41 were used for this study. Excision of the Neo resistance cassette was done at the chimera level, by breeding chimeras directly with C57BL/6 Cre deleter mouse line. F1 C57BL/6 Cre progeny were genotyped from mouse-tail lysates, using Ef and Er primers (outside of targeted exons), Wr and Wf (inside targeted exons), Nr and Nf (inside the Neo cassette) and Lxr (probing the loxP site). Details about primers and genotyping results are given in tables S5, S6 and fig. S10A. Analysis of PCR product patterns was performed by using HT DNA 5K LabChip®90 kit on the LabChip®90 microfluidic electrophoresis apparatus. A representative genotyping picture is shown in fig. S10B.

Antibodies

The primary antibodies were as follows: anti-InlC (R134, 8); anti-ActA (R32, 9) and anti-LLO (R176, 10) rabbit polyclonal antibodies; anti-V5, anti-V5-HRP and anti-V5-FITC mouse monoclonal antibodies (R960-25, R961-25 and R963-25, Invitrogen); anti-GST mouse monoclonal antibody (71097, Novagen); anti-HP1γ mouse monoclonal antibody (2MOD-1G6-AS, Euromedex); anti-BAHD1, H3, H4, KAP1, HDAC1 and HDAC2 rabbit polyclonal antibodies (ab46573, ab1711, ab7311, ab10483, ab7028 and ab7029 respectively, Abcam); anti-protein C mouse monoclonal antibody, clone HPC4 (11814508001, Roche); anti-H3K9Ac rabbit polyclonal antibody (9671, Cell Signaling Technology). The anti-LntA rabbit polyclonal antibody was generated and purified against recombinant GST-LntA as described (11). It was used at a 1:1,000 dilution in immunoblots. Secondary antibodies were Cy3-conjugated goat

anti-mouse IgGs (115-167-003, Jackson IR) for immunofluorescence (1:500 dilution), and HRP-conjugated goat anti-mouse or anti-rabbit IgGs (172-1011 or 172-1019, Bio-Rad) for immunoblots (1:10,000 dilution).

Yeast two-hybrid (Y2H) screening

The bait construct was the *lntA* gene cloned in pB27, a Y2H vector optimized by Hybrigenics, S.A., Paris, France (<http://www.hybrigenics.com>). pB27-*lntA* was transformed in the L40DGAL4 yeast strain (12) and Y2H screening was performed by Hybrigenics, as described (6). 107.42 millions of interactions were actually tested with the LntA bait. After selection on medium lacking leucine, tryptophane, and histidine, positive clones were picked and the corresponding prey fragments were amplified by PCR and sequenced at their 5' and 3' junctions. Sequences were then filtered and contiged as described previously (13) and compared to the latest release of the GenBank database using BLAST (14). In the LntA screening process, BAHD1 was found in 9 independent clones, with a Predicted Biological Score of A (very high confidence), as for two other preys.

Transient transfections with plasmids or oligofection with siRNA duplexes

Transient transfections of plasmids were performed as previously described (15) using lipofectamine 2000 (Invitrogen), according the manufacturer's protocol. Chemically synthesized siRNAs against *BAHD1* (S22351 and S22352 Silencer® siRNA) or *KAPI* (siGENOME SMARTpool M-005046-01) were purchased from Ambion or Dharmacon, respectively. The corresponding Silencer® Negative Control #1 siRNA (AM4611) and siGENOME Non-Targeting siRNA pool (D-001206-14) were used as controls. LoVo cells were transfected using Lipofectamine RNAiMAX (Invitrogen) following the manufacturer's instructions. Briefly, 10⁶ LoVo cells per well of a 6-well plate were first treated with a reverse-transfection protocol, using 5 µl lipofectamine RNAiMAX and 50 pmol of siRNA. This was followed by a forward transfection 30 h later, using the same amounts of siRNA and transfection agent. The silencing efficiency of these siRNAs for their targeted mRNA was tested by qRT-PCR as described below, 72 h post-transfection. Displayed BAHD1 silencing results proceed from S22351 transfection; S22352 gave comparable phenotypes, though with a weaker efficiency.

Cellular infections, entry and intracellular multiplication assays

In all invasion experiments, *Listeria* strains were grown in BHI medium to an OD₆₀₀ of 2 to 3, washed in PBS, and diluted in culture medium without serum, to achieve the required the multiplicity of infection (MOI). Bacterial dilutions were added to cell plates and centrifuged for 1 minute at 200 x g to synchronize entry (except for chromatin immunoprecipitations, for which 162 cm² cell flasks were used). After 1 h of incubation, cells were washed twice and the remaining non-invasive bacteria were killed by adding gentamicin 20 µg/ml in complete culture medium for 1 h (entry) to 15 h, 21 h or 23 h (intracellular multiplication).

Specific protocols were as follows:

(i) Quantifications of bacterial entry and intracellular multiplication by gentamicin survival assays (16). Bacterial dilutions were added to LoVo cells seeded in 24-well plates, to obtain a MOI of 20 to 40. After entry and gentamicin treatment, efficiencies of bacterial entry and intracellular multiplication were quantified by plating serial dilutions of cells lysates on BHI agar plates and determining colony-forming units (CFU). Experiments were performed in triplicates and reproduced at least three times. When applicable (fig. S8, table S3B), recombinant human IL-28A/IFN-λ2 (R&D system, 1587-IL-025) was added either 24 h before or concomitantly with gentamicin at the indicated concentrations.

(ii) **Microscopy.** C3SV40 cells were seeded on glass coverslips in six-well plates and infected or not with bacteria at a MOI of 100. After 22 h of infection, coverslips were processed for immunofluorescence analysis. As bacterial entry is mainly InlB-dependent in C3SV40 cells, for quantification experiments, we increased the number of infected cells by treating bacteria with the invasion protein InlB-Ami, which is able to efficiently associate to the bacterial surface when added exogenously, and to stimulate bacterial entry (17). After 30 minutes of incubation at 37°C, bacteria were washed twice in PBS and used for cell infection, as described above.

(iii) **RNA analysis.** Cells were seeded in six-well plates and infected or not with bacteria at a multiplicity of infection (MOI) of 20, and processed as for invasion assays. RNA samples were collected 16 to 24 h post infection. When siRNA treatment was needed, this was performed as described above, starting the reverse-transfection protocol 72 hours before recovery of infected cells (*i.e.* 56 h before infection for the reverse transfection, and 26 h for the forward transfection). Note that, for optimal siRNA treatment, cells had to be seeded at a lower density in these experiments than non-siRNA treated cells. This resulted in decreased cell-to-cell spread of bacteria. As a consequence, the observed effects of infection on the expression of IFN genes and ISGs were less pronounced for siRNA treated cells, in control as well as in targeted depletion samples. U-937 and THP-1 monocytes were pre-activated by adding 1 mg/ml PMA (phorbol-12-myristate-13-acetate, Sigma) to the culture medium, 24 hours before infection.

(iv) **Chromatin Immunoprecipitations (ChIP).** LoVo cell monolayers in 162 cm² flasks were infected with *IntA*- or *IntAV5+* strains at a multiplicity of infection (MOI) of 25. After 16 h of infection, cells were washed in PBS and fixed with 1% formaldehyde in PBS as described (18). For microscopy, RNA and ChIP experiments, we controlled the efficiency of infection by CFU counts on lysed cells, and by immunofluorescence using anti-*Listeria* antibody. Bacterial recovery of the *IntA*-expressing or -deficient strains proved to be very similar in every condition tested, thus excluding potential effects of bacterial load/entry/survival/proliferation variations on the described phenotypes.

Animal infections

Animal experiments were performed according to the Institut Pasteur guidelines for laboratory animal husbandry, which comply with European regulations.

(i) ***In vivo* virulence assay in BALB/c mice.** 8-week-old female BALB/c mice (Charles River) were injected intravenously with *L. monocytogenes* strains to be tested. Groups of 4 (for organs) to 6 (for blood) mice were injected with an inoculum of 8. 10³ CFU per tested strain, and sacrificed 48 or 72 h after infection. Spleens and livers were aseptically removed and separately disrupted in phosphate-buffered saline (PBS). 100 µl of blood was recovered and heparin (250 units/ml) was added to prevent coagulation. Serial dilutions of organs homogenates or blood were plated on BHI agar plates and CFU determined. Statistical analyses were performed using Student's two-tailed T-test on CFU counts. A p-value $p < 0.05$ (*) was considered statistically significant.

Note that, when we assayed the virulence of the Δ *IntA* mutant strains, comparable results were obtained with clone BUG2168 (fig. 1B and 3C) and with BUG2169 (not shown).

(ii) ***In vivo* virulence assay in *BAHDI*^{+/+} or *BAHDI*^{+/-} mice.** Six mice carrying the *BAHDI* KO (knockout) allele on one chromosome (*BAHDI*^{+/-}) and six of their littermates carrying the wild type (WT) allele (*BAHDI*^{+/+}) were used in this study. Each group contained 5 males and 1 female, all in the C57BL/6 background. These mice were injected intraperitoneally with WT EGDe. Due to resistance of C57BL/6 mice to infection by *L. monocytogenes* (19), we used an inoculum of 5. 10⁴ CFU per animal. Mice were sacrificed 72 h after infection, and CFU were enumerated in organs as described in (i).

(iii) *In vivo* RNA analysis. Bacteria were isolated from mouse spleens as previously described (20). Briefly, 6-8 weeks old specific pathogen-free female CD1 mice (Charles River) were intravenously infected with 10^6 *L. monocytogenes* EGDe bacteria. 48 h post-infection, spleens were harvested and homogenized in ice-cold solution (0.2 M sucrose, 0.01% SDS). The homogenate was gently centrifuged for 20 minutes at 300 rpm and filtered. The tissue suspension was centrifuged for 20 minutes at 4000 rpm to pellet the bacteria.

Immunofluorescence analysis, live-cell imaging and image processing

(i) For microscopy on fixed samples, cells were fixed 20 minutes at room temperature with 4% paraformaldehyde in PBS, permeabilized with 0.5% Triton X-100 in PBS for 4 minutes at room temperature, and then blocked in PBS containing 1% BSA (Sigma). Slides were then incubated either with FITC-conjugated anti-V5 for 1 hour or, when co-localizations of LntA-V5 with BAHD1-YFP was needed, with primary anti-V5 for 1 hour and then with Cy3-conjugated secondary antibody and DAPI for 30 minutes. Bacteria were visualized in phase contrast and with DAPI.

(ii) For live cell imaging, images were acquired with the microscope equipped with a temperature-controlled stage and an objective heater (Biotechs). Fluorescent illumination was driven by an ultrahigh-speed wavelength switcher Lamda DG4 (Sutter Instrument) equipped with a 175W xenon arc lamp and excitation filters for CFP and YFP (Chroma Technology). Emission filters were selected using a high-speed Lamda 10 filter wheel (Sutter Instrument).

Preparations were observed with a Zeiss Axiovert 200M epifluorescence microscope (Carl Zeiss MicroImaging, Inc.), connected to a cooled CCD camera (CoolSNAP_{HQ}, Photometrics). Images were acquired with apochromat 63x or 100x (NA 1.4) objective lenses and processed with the MetaMorph software, version 6.1 (Universal Imaging Corp., Downingtown, PA).

To quantify LntA signals in nuclei of C3SV40 cells infected with *lntA-V5+*, a region encompassing the surface of each nucleus, corresponding to the DAPI staining, was created in MetaMorph. FITC Fluorescence intensity (average intensity, expressed in arbitrary units, a.u.) was then measured in the selected area, in the image corresponding to the LntA-V5 staining. V5-specific FITC staining was compared with the background FITC staining in C3SV40 cells, or cells infected with the control strain *lntA-*. Data were gathered from 26 nuclei in three independent experiments, and background levels, collected from cell-free areas of the coverslip, were subtracted. Acquisition parameters and background levels were similar same for all samples.

Bacterial extracts, SDS-PAGE and immunoblots

Bacterial total extracts or culture supernatants were recovered from 1 ml of *Listeria* strains grown to a OD₆₀₀ of 2.0 in BH1 medium at 37°C, under microaerobic conditions. After centrifugation at 8,000 x g, the bacterial pellet was resuspended in 100 µl 2x concentrated protein electrophoresis sample buffer (SB2X, 2I), sonicated 5 times 15 seconds, and boiled for 5 minutes at 95°C. Supernatants were filtered on 0.2 µm filters, precipitated with 16% TCA for 30 minutes at 4°C and by centrifugated for 15 minutes at 4°C. The precipitated proteins were washed with acetone, and denaturated in 100 µl SB2X. 10 µl of each sample were separated by electrophoresis on 14% sodium dodecyl sulfate-polyacrylamide gels (SDS-PAGE). Proteins were detected by immunoblot using Hybond-P PVDF membranes (GE Healthcare) and a detection kit (Pierce).

GST-pulldowns

To prepare nuclear extracts, 4.10⁷ HEK293 cells transfected or not with pcDNA3.1/V5-His-TOPO-*mCFP*, or pcDNA3.1/V5-His-TOPO-*BAHD1* were harvested and proceeded with a

Nuclear Extraction Kit (Active Motif), following manufacturer's instructions. Nuclear and cytoplasmic extracts were stored at -80°C . GST-LntA or GST were produced from BL21(DE3) transformed with pET41a plasmids. 300 ml of cultures at $\text{DO}_{600} = 0.6$ were stimulated 4 h with 0.5 mM IPTG. Bacterial pellets were lysed with a French Press (13,000 PSI) in lysis buffer (15 mM HEPES pH 8.0, 100 mM NaCl, 1 mM EDTA, 1 mM DTT) supplemented with Complete protease inhibitor cocktail, EDTA-free (Roche). For pull down assays, 100 μl of a 50% slurry of glutathione sepharose 4B beads (Amersham, Biosciences) were mixed for 4 h at 4°C with bacterial lysates and processed according to the manufacturer's instructions. The amount of GST fusion proteins was estimated by either immunoblot or Coomassie brilliant blue staining for normalization of quantities used in pulldown assay. 50 μl of purified nuclear extract containing BAHD1-V5 or CFP-V5 were mixed with appropriated quantities of GST fusion protein resin in supplemented binding buffer and incubated overnight at 4°C . The beads were then washed twice with the same binding buffer and once with binding buffer without protease inhibitor cocktail. 20 μl of SB2X was added and the mixture was denaturated for 6 minutes at 100°C . After centrifugation at $2,500 \times g$ for 5 mn, 15 μl of the supernatant was subjected to SDS-PAGE and immunoblot as described above.

Expression and purification of LntA for cristallography

E. coli BL21(DE3) were transformed with pGEX-LntA plasmid. Cultures were grown at 37°C to $\text{OD}_{600} = 0.8$, then expression was induced by addition of 1 mM IPTG for 21 hours at 25°C . Cells were disrupted by sonication in PBS buffer pH 7.3 supplemented with 140 mM NaCl, protease inhibitors, DNaseI (Sigma) and RNase (Roche). The sample was centrifuged at $30,000 \times g$ for 1h 30 min, and the supernatant was loaded onto a 5 ml GStrap-HP column (GE Healthcare) equilibrated in PBS buffer. The GST-LntA₃₄₋₂₀₅ fusion protein was eluted with 20 mM reduced glutathione in 50 mM Tris-HCl, pH 8.0. After dialysis into a buffer containing 25 mM Tris-HCl pH 8.3 and 0.2 M NaCl, the GST-tag was cleaved for 6 hours with 0.5 U of thrombin/mg of protein. The digested sample was reloaded onto the GStrap-HP column and the unbound fraction was loaded onto a Superdex 75 column equilibrated in 25 mM HEPES, 0.1 M NaCl, 1 mM EDTA, pH 7.5. The selenomethionine form of LntA was expressed in minimal medium and purified as for the native protein, except that 5 mM DTT was added to the GST equilibration buffer and an additional MonoQ HR5/5 step was performed at pH 8.0 before gel filtration. Mass spectrometry confirmed the full substitution of the three methionines.

Crystallization, structure solution and refinement

Purified LntA₃₄₋₂₀₅ was concentrated to 10 mg/ml, and an initial screening using the high throughput crystallization platform of the HTXLab (PSB, Grenoble, France) performed at 4°C yielded more than 100 different hits. Several crystal forms were reproduced by hand at 20°C . The best crystals grew in 2 months in 0.15 M NaSO_4 , 18% PEG 3350 and, before data collection, were cryoprotected by successive incubation in mother liquor containing increasing concentrations of glycerol (up to 25%).

A SAD-dataset on the Selenium edge was collected on BM30A at the ESRF-Grenoble to a resolution up to 2.3\AA . Data were indexed (space group $P4_12_12$) and scaled with the XDS package (22). Heavy atoms sites, refinement and phasing were performed by AutoSHARP (23, 24). Cycles of intercalated automatic and manual building were performed using ARP/wARP and Coot (25, 26), coupled with refinement cycles by REFMAC 5.4 (27). Data collection and refinement statistics are shown in table S7.

The LntA molecular structure data are deposited at the Worldwide Protein Data Bank (<http://www.wwpdb.org/>), ID #2xl4, structure factor file #r2xl4sf.

Tandem affinity purification of the HPT-BAHD1-associated complex and mass spectrometry analysis

We carried out a double-affinity purification of HPT-BAHD1 from HEK293-HPT-BAHD1 cells, or a negative control purification from HEK293-HPT-blue cells, starting from 7.5 g of frozen cellular pellet. Preparation of nuclear soluble and chromatin fractions was as described (28). HPT-tagged BAHD1 associated complexes were then purified by two-step affinity chromatography using (i) Anti-Protein C Affinity Matrix (Roche) for the binding of the protein C epitope and (ii) Ni Sepharose High Performance (GE Healthcare) for the binding of the His₆-tag. Since the recognition of the protein C epitope by the HPC4 antibody is calcium-sensitive, no EDTA was added in the first chromatography step. Instead, TGN binding and wash buffer (20 mM Tris pH 7.65, 10% glycerol, 150 mM NaCl, 0,01% Igepal) was supplemented with 1 mM CaCl₂. After overnight binding to the resin, bound complexes were extensively washed, and then eluted with TEGN (TGN, 5 mM EGTA, pH 7.65). Eluates were supplemented with 30 mM imidazole and further affinity-purified on Ni-sepharose. After 2 h of binding to the resin, bound complexes were extensively washed with TIGN (TGN, 30 mM imidazole, pH 7.65), and eluted with 2X NuPAGE LDS sample buffer (Invitrogen). Double-immunopurified complexes were resolved on NuPAGE Novex 4-12% Bis-Tris gels in MOPS buffer (Invitrogen). For the analytical gels (fig. 2C and S6A), we loaded 1/100th of the eluate from the 1st column, and 1/10th of the eluate from the 2nd column, and stained with the SilverQuest staining kit (Invitrogen). For control immunoblots, we loaded 1/1,000th and 1/100th of the two eluates, respectively, and 1/10,000th of the input and flow through fractions. For the preparative gel (fig. S6B), we loaded 1/4th of the eluates from the 1st and 2nd columns, and stained with Colloidal Blue staining kit (Invitrogen). Bands were cut out from the two-spep purified complex lane for mass spectrometry (MS) analyses (see below).

NanoLC-MS/MS analyses for protein identification

Standard enzymatic digestion of excised bands was performed with trypsin (Gold Promega 10ng/μl) using the Progest robot (Genomic Solutions). Peptide mixtures were SpeedVac-treated for 10 min then solubilized with 0.1% formic acid and injected in a Q-TOF Premier mass spectrometer coupled to a nanoAcquity liquid chromatography equipped with a trapping column (Symmetry C18, 180 μm × 20mm, 5 μm particle size) and an analytical column (BEH130 C18, 75 μm × 100 mm, 1.7 μm particle size) (Waters). The aqueous solvent (buffer A) was 0.1 % formic acid in water and the organic phase (buffer B) was 0.1 % formic acid in acetonitrile. A 2-40% B gradient was set for 25 min. For exact mass measurements, glufibrinopeptide reference ($m/z = 785.8426$) was continuously supplied during nanoLC-MS/MS analyses using the lockspray device. Peptide mass measurements were corrected during data processing and peak lists were generated by PLGS (ProteinLynx Global Server, Waters). Processed data were submitted to Mascot searching using the following parameters: data bank NCBI; taxonomy Human; peptide tolerance 20 ppm; fragment tolerance 0.1 Da; digest reagent trypsin with one missed cleavage allowed; variable modifications oxidation (Methionine) and fixed modifications carbamidomethylation (Cysteine). Validation criteria for protein identification were: two peptides with a Mascot individual ion score >30.

Sandwich ELISA measurement of mouse IFN-λ3 in organ homogenates

Mouse liver and spleen homogenates were prepared as described in the Animal infections section (i). Concentrations of IFN-λ3 in homogenates was determined using Mouse IL-28B/IFN-lambda 3 DuoSet (DY1789, R&D Systems), according to the manufacturer's instructions. Briefly, wells of a 96-well plate were pre-coated with specific rat anti-mouse IL-28B capture antibody and saturated with PBS, 1% BSA (Reagent Diluent). 1 ml of each organ

homogenate was clarified by two successive centrifugation steps at 1,000 and 10,000 x g, respectively. 30 µl of sample supernatants from three distinct biological replicates were added to wells of the prepared ELISA plate, pre-filled with 70 µl of Reagent Diluent. A standard curve was included, by loading in wells 100 µl of 2-fold serial dilutions of recombinant mouse IL-28B, starting from 2 ng/ml. After thorough washing steps, the detection antibody was then added, followed by the streptavidin-HRP conjugate, as specified by the manufacturer. Signals were revealed with Substrate and Stop Solutions (DY999 and DY994 respectively, all from R&D Systems), and detected by reading the Absorbance at 450 nm using a TriStar LB941 device (Berthold technologies). For wavelength correction, readings at 590 nm were subtracted from the obtained values. Statistical analyses were performed using Student's two-tailed T-test on calculated concentrations.

Bacterial RNA extraction and qRT-PCR

RNA samples from *Listeria* grown to exponential or stationary phase at 37°C in rich medium or extracted from mouse spleens were extracted as previously described (20, 29) and treated with TURBO DNA-free™ kit (Ambion).

Bacterial cDNAs were generated with iScript cDNA Synthesis kit (Bio-Rad), following the manufacturer's protocol. Quantitative real-time PCR (qRT-PCR) was performed on a MyIQ device (Bio-Rad). Classical runs were 45 cycles with a hybridization temperature of 60°C. Each reaction was performed in triplicate. 2 µl of diluted cDNA samples were mixed with 10 µl of SYBR® Green PCR master mix (Bio-Rad) and 0.25 pM (each) forward and reverse primers in a final volume of 20 µl. A standard curve was generated for each primer pair by using three ten-fold dilutions of a PCR product of defined concentration, to ensure that PCR efficiency was 100%. Data were analyzed by the $\Delta\Delta C_t$ method. Target gene expression data were normalized by the relative expression of a reference gene (*16S rRNA* or *gyrA*). The expression of the control *lmo2845* gene, which encodes a putative transmembrane efflux protein, was not affected *in vivo* (20). The neat concentration of cDNA molecules in samples was calculated using standard curves. The specific primers pairs for each bacterial gene are specified in table S5.

Transcriptome analysis of infected cells

RNA from LoVo cells grown in 6-well plates and infected with either *lntA*^{V5+} or *lntA*⁻ strains was extracted using the RNeasy Mini Kit (Qiagen). Three biological replicates were analyzed for each experimental condition. RNA quality was monitored on Agilent RNA Pico LabChips (Agilent Technologies, Palo Alto, CA). 300 ng of total RNA were analysed using the Affymetrix Human Gene1.0 ST Array (exon array), according to the GeneChip whole transcript sense target labeling assay manual, using the GeneChip WT cDNA Synthesis and amplification Kit and WT terminal labeling Kit. Human Gene 1.0 ST array interrogates 28,869 well-annotated genes with 764,885 distinct probes. The RNA was reverse transcribed using random primers tagged with a T7 promoter sequence. The second strand was synthesized, and the dsDNA was used as a template and linear amplified by T7 RNA polymerase. The cRNA was reverse transcribed using a mixture of dNTPs and dUTP and random primers. After RNaseH digestion, the ssDNA was fragmented with a combination of Uracil DNA glycosylase and apurinic/aprimidinic endonuclease 1. The fragmented ssDNA was end-labeled by terminal deoxynucleotidyl transferase with the Affymetrix proprietary DNA labeling reagent, which is covalently linked to biotin. The fragmented and labeled ssDNA was hybridized to arrays for 18 h and washed and scanned with the Affymetrix wash station and scanner. For data analysis, cell intensity files were generated with GeneChip Operating Software. Raw data were processed by the Robust Multichip Analysis (RMA) algorithm. A test for differential expression was performed between these two groups using the "lpe" package available on the R-open source

software platform. Genes were considered to be significantly differentially expressed with a p-value of < 0.05 after multiple testing correction (Benjamin-Hochberg).

Complete data are deposited in the Gene Expression Omnibus Database (<http://www.ncbi.nlm.nih.gov/geo/>) with GEO accession number GSE26414.

Human and mice RNA extraction and qRT-PCR

RNA from infected and/or siRNA-treated human cells was extracted using RNeasy Mini Kit (Qiagen), using 1 column per well of a 6-well plate. For RNA extraction from mice kidneys, each organ was disrupted directly in 1 mL RLT buffer supplemented with β -mercaptoethanol using a GentleMACS Dissociator (Miltenyi Biotech). 100 μ L of organ homogenate was diluted in 250 μ L RLT buffer before loading on a RNeasy Mini column and processing to extraction as recommended by the manufacturer.

Genomic DNA was removed by treatment with TURBO DNA-free™ kit (Ambion). cDNAs were generated from 1 to 2 μ g total RNA using the RT² first strand kit (SABioSciences), and quantitative PCR was performed with RT² qPCR Primer Assay (SABioSciences) following the manufacturer's protocol and the recommended two-step cycling program, on a MyIQ device (Bio-Rad). Each reaction was performed in triplicate. All human and mice qRT-PCR primers were pre-designed, validated RT² qPCR primer pairs from SABioSciences. Data were analyzed by the $\Delta\Delta$ Ct method. Target gene expression data were normalized to the relative expression of the *GAPDH* reference gene. Similar results were obtained when *HPRT1* transcript was used as a reference.

Chromatin immunoprecipitation experiments and site-specific PCR analysis

This protocol was adapted from Boukarabila *et al.* (18). Chromatin inputs corresponding to 3.10⁶ cells were used for each individual BAHD1 or H3K9Ac ChIP assay, and 1.10⁶ cells for H3 ChIPs. All buffers were supplemented with Complete EDTA-free protease inhibitor cocktail tablets (Roche). Formaldehyde-fixed cells were washed in PBS and lysed in 10 mM Tris, pH 8, 10 mM EDTA, 0.5 mM EGTA, 0.25% Triton X-100 for 5 min on ice. The nuclear pellets were recovered by brief centrifugation at 3,000 x g, and the soluble nuclear fraction was extracted with 250 mM NaCl, 50 mM Tris pH 8, 1 mM EDTA, 0.5 mM EGTA for 30 min on ice. After brief centrifugation at 16,000 x g, the chromatin pellets were resuspended in 10 mM Tris pH 8, 1 mM EDTA, 0.5 mM EGTA, 0.5% SDS, and then sonicated with a Bioruptor (Diagenode) to shear chromatin to a final size of 150-600 bp. Extracts were quantified by A_{260nm} measurement, and material quantities were adjusted accordingly. Samples were then diluted to obtain the following IP buffer composition: 150 mM NaCl, 10 mM Tris pH 8, 0.1% SDS, 1% Triton X-100, 0.1% sodium deoxycholate, 1 mM EDTA, 0.5 mM EGTA. IP was carried out overnight at 4 °C with anti-BAHD1, -H3K9Ac or control -histone H3 antibodies. The immunocomplexes were recovered with Dynabeads Protein G (Invitrogen) added for 90 min and then washed 5 times in a succession of isotonic and saline buffers as described (18). After a final wash in 10 mM Tris pH8, 1mM EDTA, 0.01% Igepal, bound material was eluted by the addition of water containing 10% Chelex (Bio-Rad), followed by boiling for 10 min to reverse the crosslink. Samples were then incubated with proteinase K (100 μ g/mL) for 30 min at 55 °C with some shaking, and then boiled for another 10 min. Finally, the ChIP DNA fraction was separated from beads and Chelex matrix by centrifugation. The recovered supernatants were quantified by qRT-PCR, performed in triplicates in the same conditions as described above for bacterial cDNA quantifications; data analysis was performed with the $\Delta\Delta$ Ct method. All primer sequences are given in table S5. The IFITM1-e1 primer pair amplified a 127 base-pair region located in the first exon of the gene, just downstream of the ISRE (Interferon Stimulation Response Element). CD44-GpG, IGF2-P3b and IFIT3-TS primer pairs were described

previously (6, 30). All PCR efficiencies, calculated on serial dilutions of purified input DNA, were 90%–100%. The qRT-PCR values obtained for the recruitment of the BAHD1 or H3K9Ac antibodies to chromatin were normalized using histone H3 antibody ChIP signals on the same chromatin extract as a reference.

SOM text

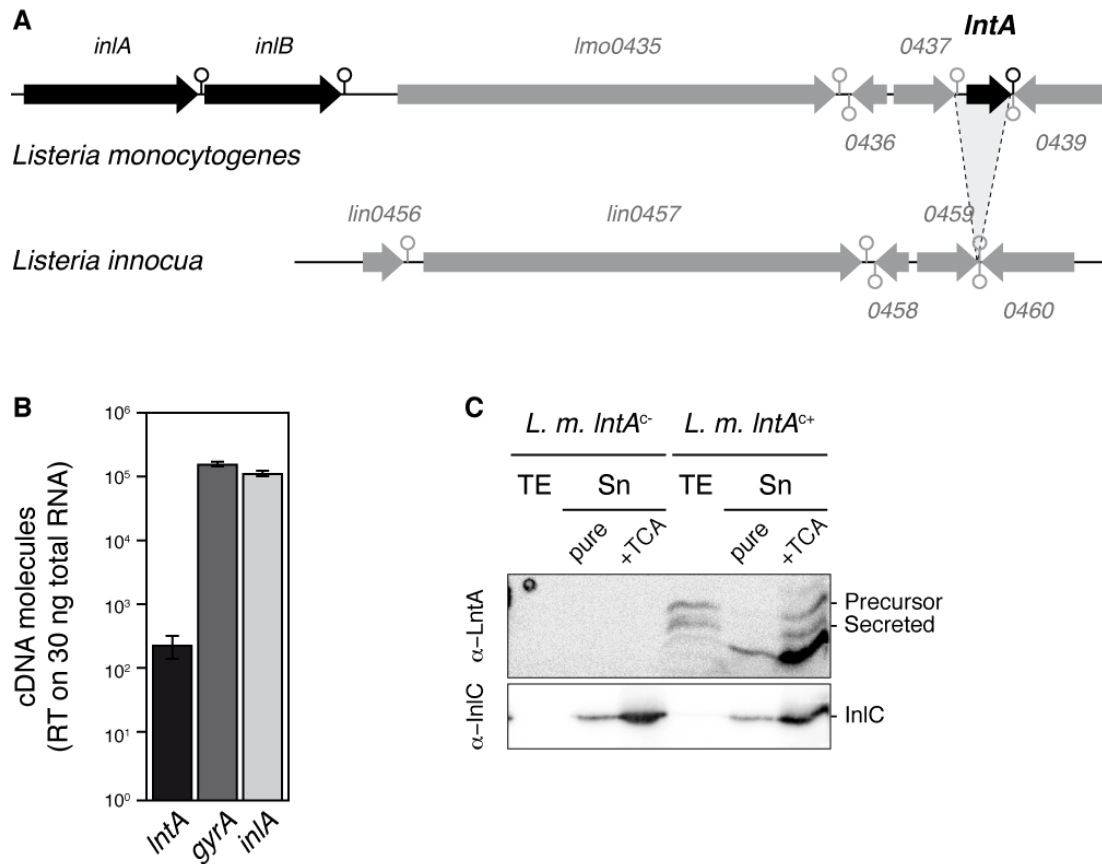
Roles of type I, II and III interferons in listeriosis

Type I interferons are beneficial for *Listeria*, while type II interferons are highly detrimental for this pathogen (31, 32). In the context of viral infections, IFN-III have been reported to substitute for type I IFN in specific tissues, such as epithelia (33, 34). We propose that LntA-mediated expression of ISGs downstream of IFN-III may be beneficial for *Listeria* only at a certain time of the infection and in specific cells.

Influence of the genetic background on the outcome of murine listeriosis

To address the role of BAHD1 in murine listeriosis, we have generated *BAHD1*^{+/-} mice. For technical reasons, we had to generate these mice in the C57BL/6 background, which is much more resistant to *Listeria* infection than the BALB/c background (19). This explains why CFU counts in organs were several orders of magnitude lower for experiments in *BAHD1*^{+/-} mice and their WT littermates than in BALB/c mice (compare fig. 1B and 3C to fig. 3D).

Supporting Figures

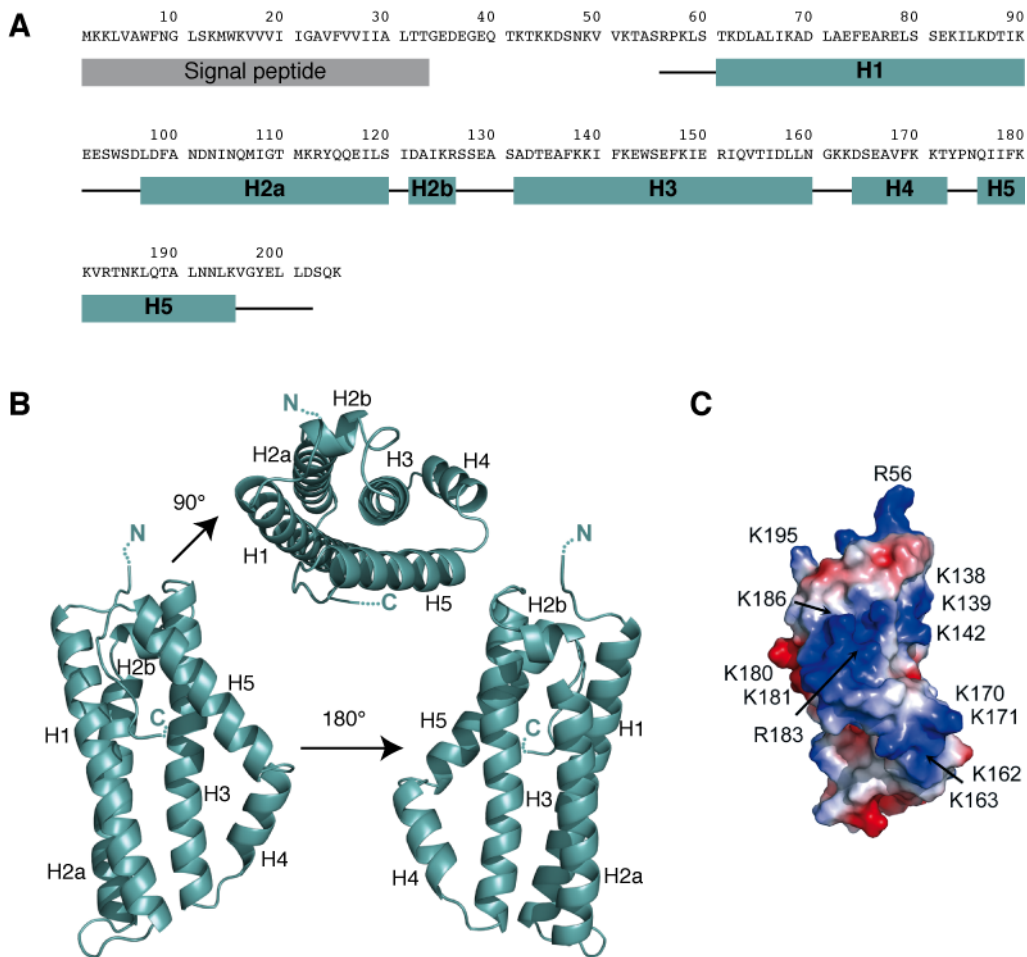
Fig. S1. Identification of *lntA* as a candidate virulence gene encoding a secreted protein.

(A) The *lntA/lmo0438* genome region in *L. monocytogenes* aligned with the corresponding region in the *L. innocua* genome. Genes with PrfA and σ_B boxes are in black. *lmo0438* was selected as a candidate virulence gene by a genome-based *in silico* approach. Bioinformatic prediction of protein export signals had identified 138 genes encoding putatively secreted proteins in *L. monocytogenes* EGDe, e.g. proteins containing putative secretion signals and no domain for association at the bacterial surface (35). Further analysis of surface proteins allowed us to reduce this number to 121 (36). Among them, 22 genes were absent in the non-pathogenic *L. innocua* species (1), of which 6 known virulence genes, such as *hly*. We selected *lmo0438* from the 16 remaining genes, because it localizes in the vicinity of the *inlAB* operon, which encodes major invasion proteins, and because *lmo0438* promoter region displays recognition boxes for PrfA and σ_B . These two regulators of virulence genes play key roles in the *L. monocytogenes* transition from saprophytic to pathogenic life (37, 38).

(B) *lntA* is expressed at very low levels by the *L. monocytogenes* EGDe strain grown in rich medium, when compared to the housekeeping gene *gyrA* or the virulence gene *inlA*. *lntA* thus behaves as a category of *Listeria* virulence genes that are not expressed in broth or tissue-cultured cells and are induced *in vivo*, such as *inlJ* (39). *lntA*, *inlA* and *gyrA* cDNA molecules were quantified by qRT-PCR, thanks to a standard curve performed on PCR products of known concentration. Data were normalized to 30 ng of starting total RNA, extracted from WT *Listeria* grown to stationary phase in BHI medium, under microaerobic conditions.

(C) *lntA* encodes a secreted protein. *L. monocytogenes* constitutively expressing *lntA* from a *P_{HYP}ER* promoter integrated on the bacterial chromosome (*lntA_{c+}*) or *L. monocytogenes* with the integrated empty vector (*lntA_{c-}*), were grown at 37°C in BHI to a OD₆₀₀ of 2. Proteins from the bacterial total extracts (TE) and the supernatant fraction (Sn, pure or precipitated with TCA) were analyzed by immunoblot with antibodies against LntA and InlC, used as control of a secreted protein. The precursor protein (~23.4 kDa) is present in TE. The mature secreted LntA (~19,7 kDa) is present in the Sn fraction.

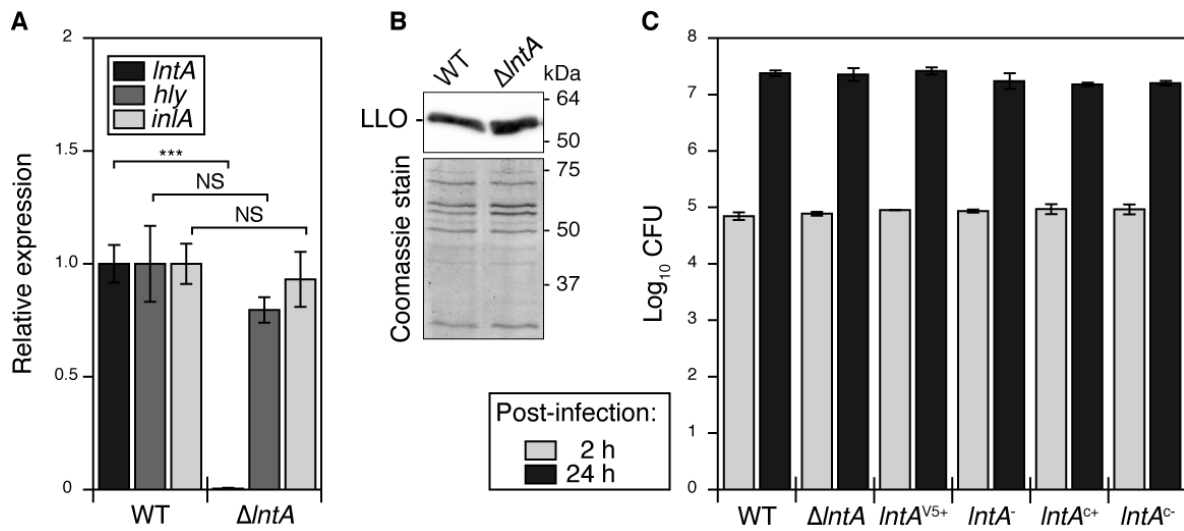
Fig. S2. LntA folds into a compact helical structure.



(A) LntA sequence. Positions of helices H1 to H5 in the secondary structure are shown below the protein sequence.

(B) Crystal structure of LntA₅₆₋₂₀₂. We crystallized LntA₃₄₋₂₀₅ and solved its structure by single anomalous dispersion (SAD) to 2.3 Å resolution (data collection and structure refinement statistics can be found in table S7). The crystallographic model contains one LntA molecule per asymmetric unit and includes residues 56-202. The five α -helices (H1 to H5) compose a compact structure. Three long central helices (H1, H2 – formed by H2a and H2b – and H3) form the core of the structure. The last two helices (H4-H5) form a right angle along the axis. Residues 34-55 and 203-205 could not be traced in the electron density map and are thus represented as dots. Structure data are deposited at the PDB (<http://www.wwpdb.org/>), ID #2x14, structure factor file #r2x14sf.

(C) Surface representations of LntA with positive (in red) and negative (in blue) charges. In addition to numerous basic residues, an acidic patch decorates the bottom of the structure.

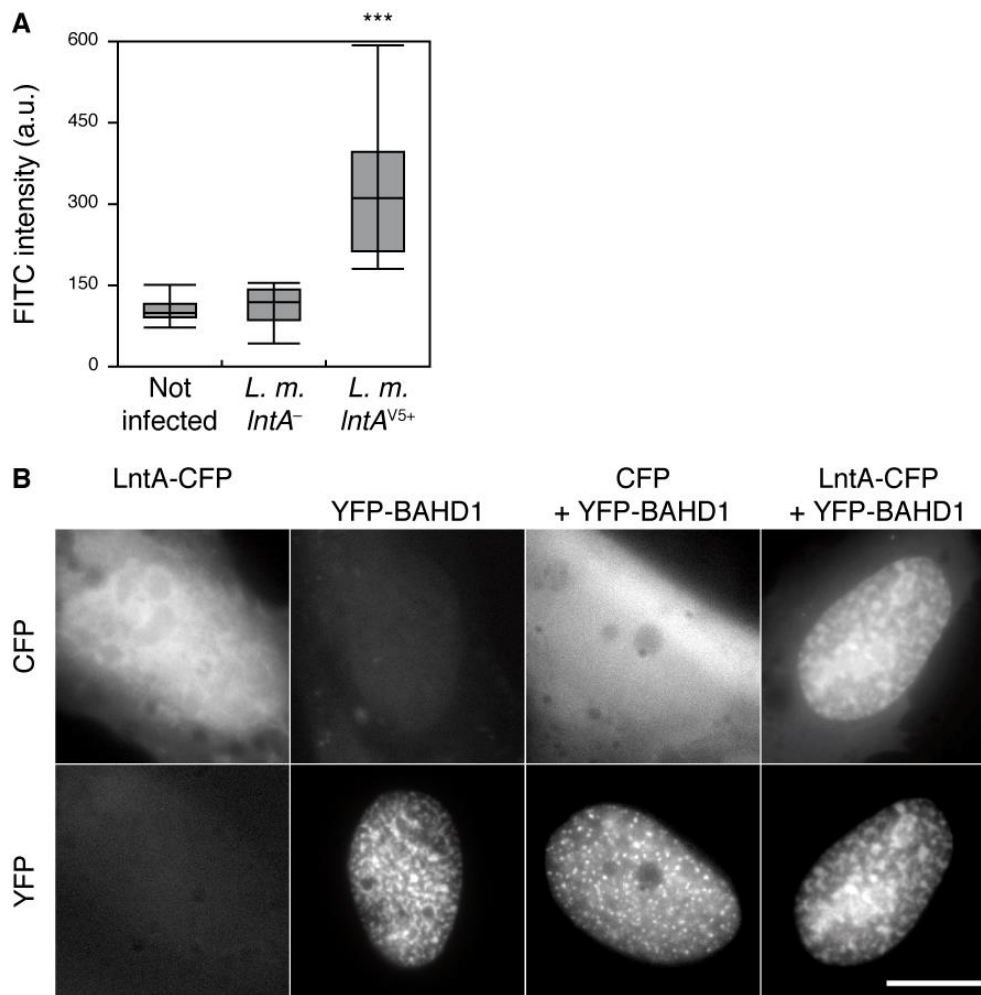
Fig. S3. Deletion or constitutive expression of *IntA* does not alter bacterial invasion of host cells.

(A) Deletion of *IntA* does not affect the expression of *inlA* and *hly* virulence genes. *IntA*, *hly* and *inlA* mRNA levels were quantified by qRT-PCR on total RNA from WT EGDe or $\Delta IntA$ isogenic strains. Data were normalized to *gyrA* mRNA and levels in WT. Error bars indicate standard deviation. Relative expression values of *hly* and *inlA* in $\Delta IntA$ strain are not statistically different (NS) from WT levels, according to a two-tailed T-test. ***, $p < 0,001$.

(B) Deletion of *IntA* does not affect the secretion of the *hly* product, listeriolysin O (LLO). WT and $\Delta IntA$ *Listeria* strains were grown in BHI to stationary phase. Proteins from culture supernatants were precipitated with TCA, then separated by SDS-PAGE on two identical gels. One gel was used for an immunoblot with antibodies against LLO (upper panel). The second gel was stained with coomassie (lower panel).

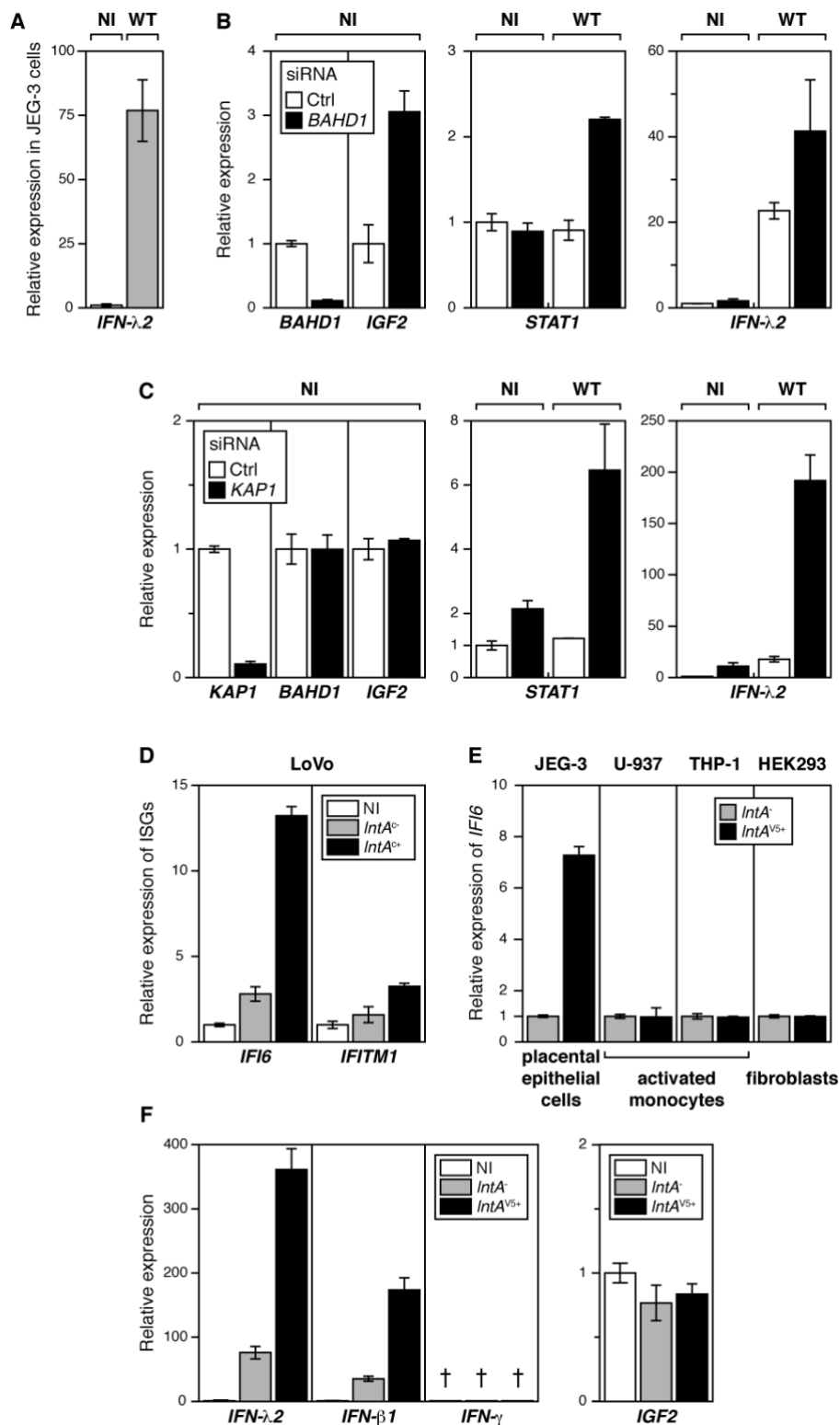
(C) Bacterial intracellular multiplication in LoVo cells is not altered by depletion or constitutive expression of *IntA*. The number of intracellular bacteria in infected LoVo cells was quantified 2 h or 24 h post infection by a gentamicin survival assay. *IntA*-expressing or non-expressing *L. monocytogenes* strains displayed no significant difference in intracellular replication in host cells.

Fig. S4. LntA colocalizes with BAHD1 in the nucleus of human living cells.



(A) Quantification of the LntA-V5 signal in the nucleus of human infected cells. C3SV40 fibroblasts were infected or not for 22 h with *lntA⁻* or *lntA^{V5+}* bacteria. The LntA-V5 protein was detected by immunofluorescence with FITC-coupled α -V5 antibody. FITC fluorescence signals were quantified in the nuclei of cells. The box-whisker plot indicates quartiles and median values. a.u., arbitrary units; ***, $p < 0.001$ (two-tailed T-test). The V5 staining was significantly more intense in nuclei of *lntA^{V5+}* infected cells compared to non-infected cells or cells infected with the *lntA*-deficient strain.

(B) Ectopically expressed LntA colocalizes with BAHD1-induced heterochromatin foci in living cells. pEYFP-BAHD1 was co-transfected into C3SV40 cells with either pE-mCFP-*lntA* or pE-mCFP. Fluorescent CFP (upper panels) or YFP (lower panels) signals were monitored in mono- or co-transfected living cells. Scale bars, 5 μ m.

Fig. S5. Expression of interferon genes and ISGs in response to *Listeria* infection.

(A) *L. monocytogenes* induces the expression of IFN-III in placental epithelial JEG-3 cells. qRT-PCR analysis of *IFN- λ 2* expression in response to *Listeria* infection of JEG-3 cells infected for 16 h with WT *L. monocytogenes* (gray), compared to non-infected cells (NI, white). All data (here and in panels B-F) were analyzed with $\Delta\Delta C_t$ method and normalized to *GAPDH* housekeeping gene transcript level.

(B) Quantification of *BAHD1*, *IGF2*, *STAT1* and *IFN- λ 2* expression levels in control or *BAHD1* siRNA-treated LoVo cells. Efficiency of the 72-h siRNA treatment was assessed by qRT-PCR. As we reported previously in HEK293 cells (6), *IGF2* expression increased upon *BAHD1* knockdown in LoVo cells. As we showed for other ISGs (fig. 2B), *STAT1* and *IFN- λ 2* expression levels were higher upon *BAHD1* knockdown in 16-h *Listeria*-infected cells.

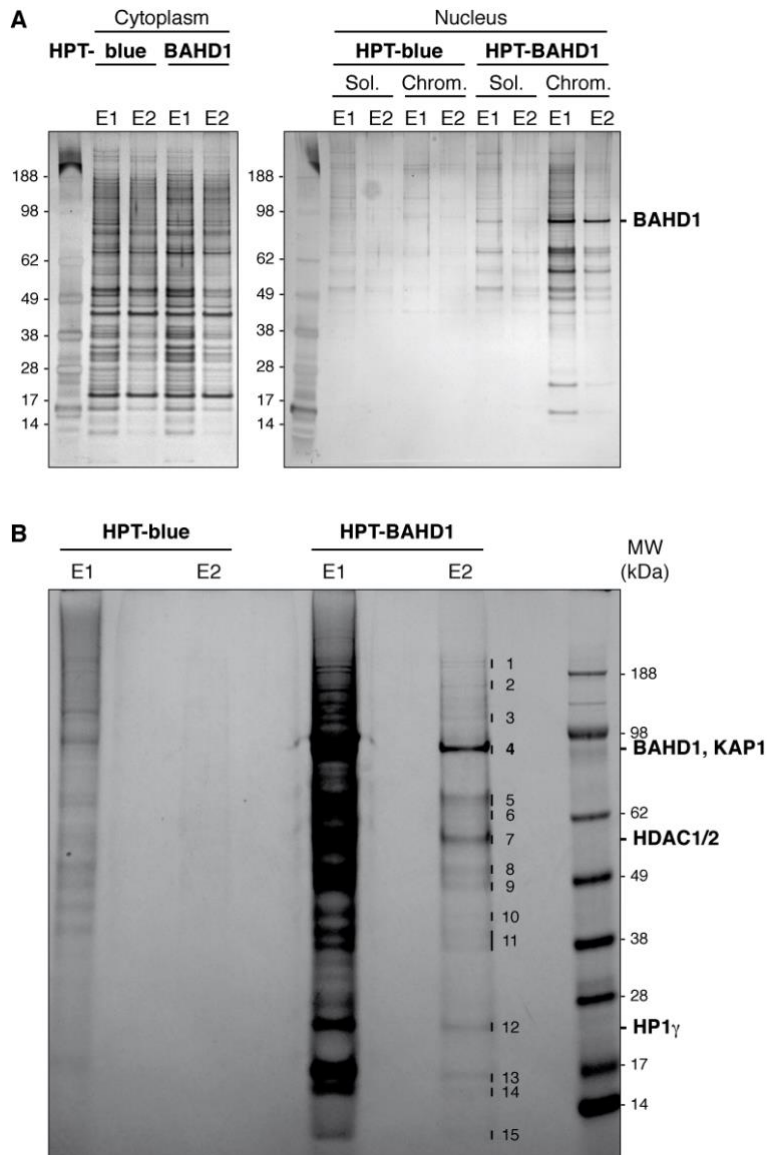
(C) Quantification of *KAP1*, *BAHD1*, *IGF2*, *STAT1* and *IFN- λ 2* expression levels in control or *KAP1* siRNA-treated LoVo cells. *KAP1* siRNA affected neither *BAHD1*, nor *IGF2* expression. *STAT1* and *IFN- λ 2* expression levels increased upon *KAP1* knockout, as for any other ISG (fig. 2B).

(D) Non-tagged LntA up-regulates ISGs in infected cells when expressed from the chromosome. *IFI6* and *IFITM1* mRNA levels were estimated by qRT-PCR on total RNA from LoVo epithelial cells infected for 22 h with either the *lntA*-deficient *lntA_c-* strain, or the isogenic *lntA_c+* strain that expressed constitutively *lntA* from a chromosomal locus.

(E) LntA up-regulates ISGs only in infected cells of epithelial origin. JEG-3, U-937, THP-1 or HEK293 cells were infected with the *lntA₋* or *lntA_{v5+}* strains for 22 h. mRNA quantifications and normalizations were as above.

(F) Right. The expression of *IFN- λ 2* and *- β 1* is stimulated by LntA, as observed for other ISGs. LoVo cells were infected with the *lntA₋* or *lntA_{v5+}* strains for 16 h, or not infected. mRNA quantifications and normalizations were as above. Note that the expression of IFN- γ remained below detection limits (\dagger), as expected in a non-hematopoietic cell lineage.

Left. Quantification of *IGF2* expression levels in infection experiments. LoVo cells infected for 16 h with either *lntA₋* or *lntA_{v5+}* *Listeria monocytogenes* were not affected for the expression of *IGF2*, compared to non-infected cells.

Fig. S6. Tandem-affinity purification of the HPT-BAHD1 associated complex.

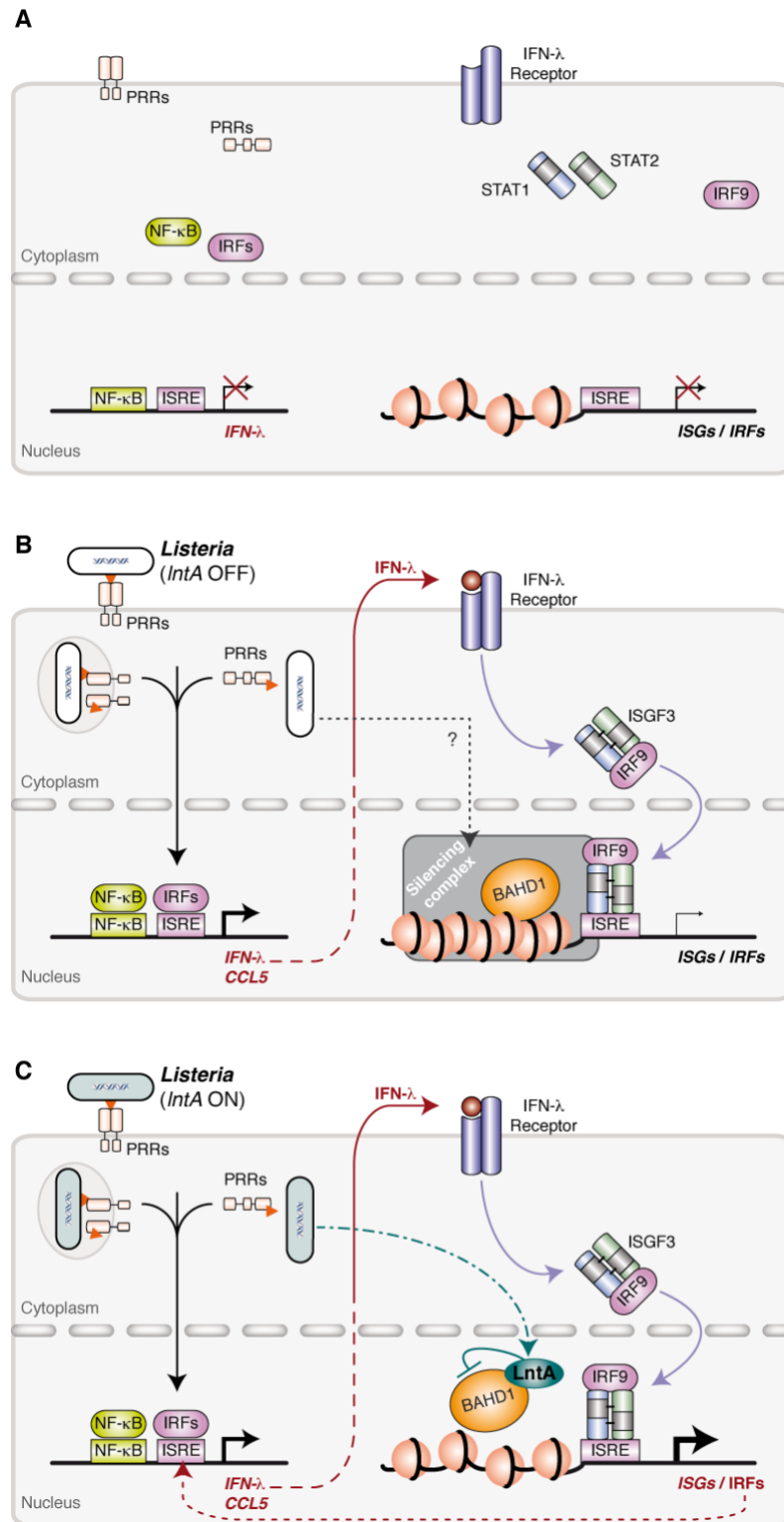
(A) BAHD1 is specifically enriched in the chromatin-associated fraction.

Cytoplasmic, soluble nuclear (Sol.) or solubilized chromatin (Chrom.) extracts of HEK293-HPT-BAHD1 cells or control HPT-blue cells were separated by two successive steps of chromatography. Eluates were separated by gradient SDS-PAGE, and stained with Coomassie colloidal staining. E1, eluted fractions from the anti-protein C resin (1/100 total); E2, eluted fraction from the nickel-sepharose resin (1/10 total).

Note that affinity-purified HPT-BAHD1 is specific of the chromatin extracts. In other fractions, recovered material is mostly non-specific, as highlighted by the comparison with HPT-blue lanes. The HPT tag consists of a His₆, protein C epitope, TEV cleavage site sequence.

(B) Preparative gel for the analysis of the HPT-BAHD1-associated complex by mass spectrometry. 1/4th of the chromatin-specific E1 and E2 eluates were separated by gradient SDS-PAGE, and stained with Coomassie colloidal staining. Bands 1-15 from the two-step purified, chromatin-associated complex were cut out and proteins were identified by LC-MS-MS. Those containing BAHD1, KAP1, HDAC1/2 and HP1 γ are highlighted.

Fig. S7. Proposed model for BAHD1/LntA-mediated regulation of ISGs.



(A) Interferon genes and ISGs are not expressed in resting cells.

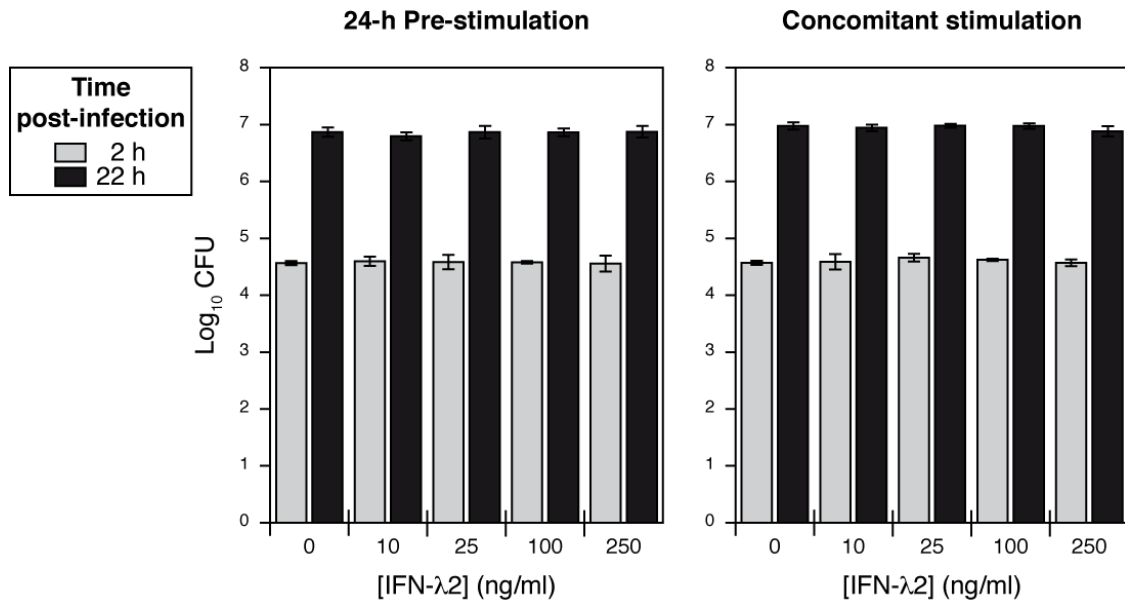
(B) During infection of epithelial cells by *L. monocytogenes*, the recognition of bacterial molecules (MAMPs, Microbial Associated Molecular Patterns) by Patterns Recognition Receptors (PRRs) activates NF- κ B and IRF transcriptional factors, which translocate into the nucleus and induce expression of type III, and to a lesser extent type I, interferons, as well as

of other NF- κ B/IRF-dependent genes, such as *CCL5*. Subsequently, IFN- λ s are secreted, activate their receptor and the downstream JAK/STAT pathway, leading to translocation of ISGF3 (*e.g.* STAT1/2-IRF9 complex) transcription factor into the nucleus. However, in response to a still non-identified infection-triggered signaling pathway, the BAHD1 silencing complex down-regulates ISGs by compacting chromatin.

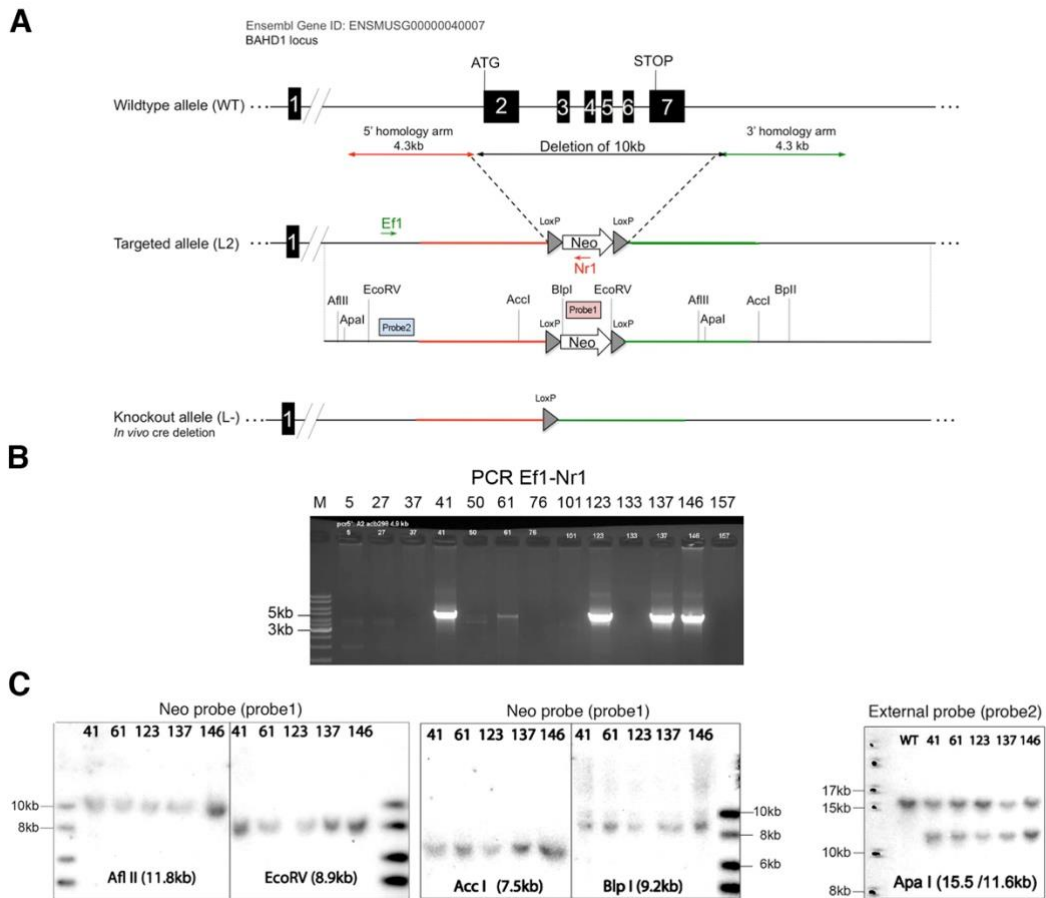
(C) Under specific conditions, *i.e.* in specific tissues and at a given time point during infection, *Listeria* secretes LntA, which enters the host cell nucleus. Binding of LntA to BAHD1 destabilizes the repressive complex and enhances expression of ISGs and IRFs genes that further amplify *IFN- λ* and *CCL5* expression.

DNA binding sites for IRFs, NF- κ B and ISGF3 are shown by boxes. Chromatin nucleosomes are shown by circles. □ MAMPs. IRF, Interferon Regulatory Factor; ISRE, Interferon Stimulation Response Element; ISGF3, Interferon-Stimulated Gene Factor-3.

Fig. S8. Bacterial intracellular multiplication in LoVo cells is not altered by IFN- λ -stimulation.



LoVo cells were pre-stimulated 24 h before infection with WT *L. monocytogenes* (*left*) or stimulated together with infection (*right*), with increasing concentration of purified recombinant IFN- λ 2. Cell response to IFN- λ 2 was checked in parallel by quantifying representative ISG transcripts by qRT-PCR (not shown). The number of intracellular bacteria in infected cells was not statistically different, with or without IFN- λ 2 treatment.

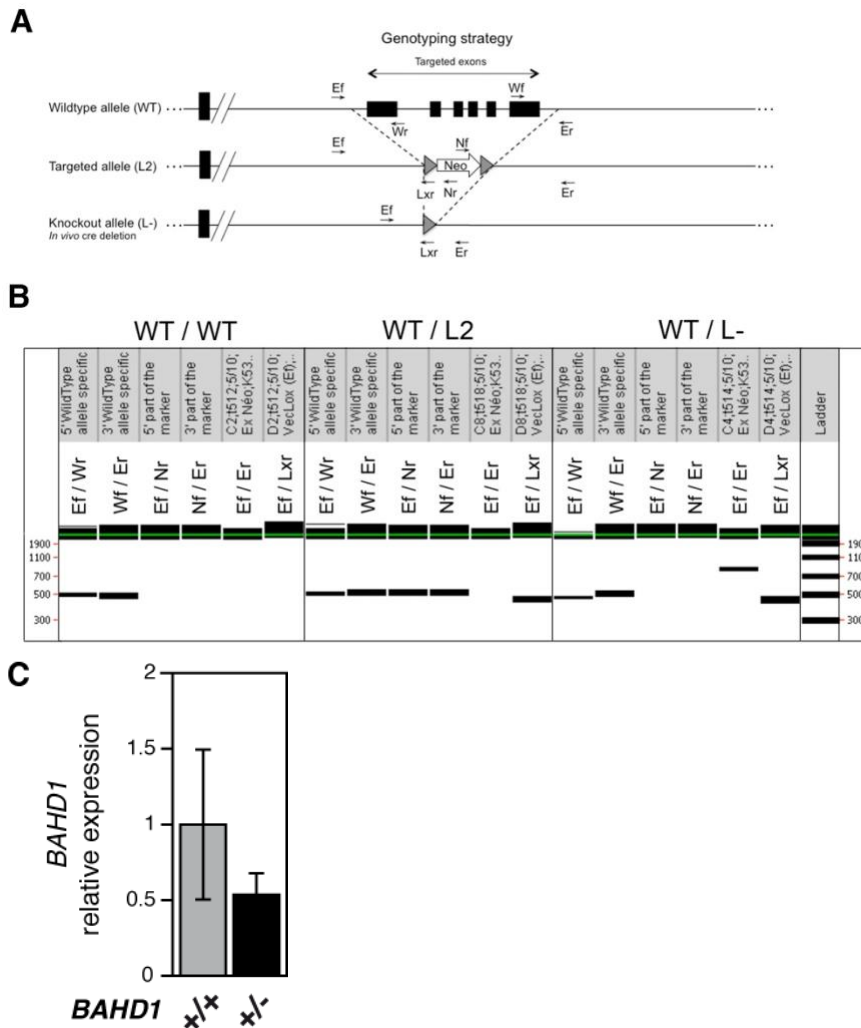
Fig. S9. Verification of the *BAHD1* KO allele.

(A) The *BAHD1* KO allele was generated by homologous recombination replacement of the entire coding region of the *BAHD1* allele (10kb) with a neomycin cassette (Neo) flanked by loxP sites, leading to the targeted allele (L2). The Neo cassette was excised upon expression of the Cre recombinase *in vivo*, leading to the knockout allele (L).

(B) PCR amplification using Efl and Nr1 primers identified 5 positive ES clones.

(C) Positive clones were further tested by Southern blotting using a Neo probe (probe1) or an external probe (probe2). The positions of the restriction sites and probes used are shown in (A).

Fig. S10. Genotyping of *BAHD1*^{+/-} mice.

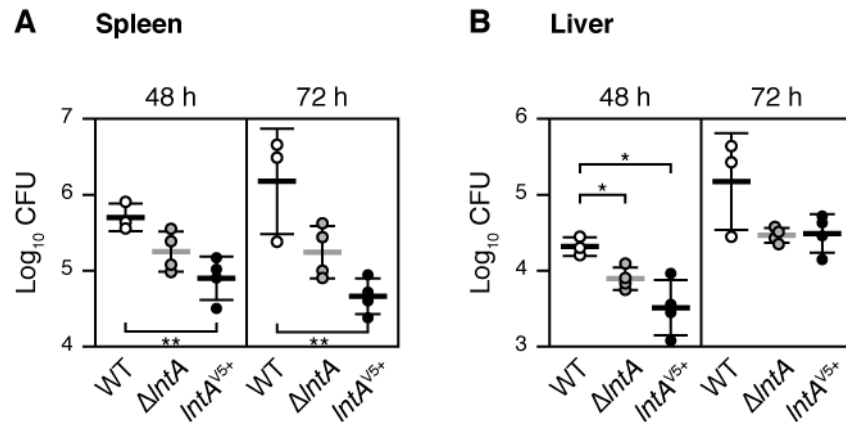


(A) The map describes the position of the primers used for genotyping for each possible allele.

(B) A representative genotyping picture obtained with LabChip®90 microfluidic apparatus. The primers used and size of expected products are shown in table S5.

(C) Expression of *BAHD1* mRNA in organs of *BAHD1*^{+/-} mice and their *BAHD1*^{+/+} littermates. *BAHD1* mRNA was quantified by qRT-PCR on total RNA extracted from mice kidneys. Data were analyzed with the $\Delta\Delta C_t$ method and normalized to *GAPDH* housekeeping gene transcript level.

Fig. S11. Both deletion and constitutive expression of *IntA* in *Listeria* decrease bacterial burden during murine systemic listeriosis.



Mice were infected intravenously with WT *L. monocytogenes*, $\Delta IntA$ or $IntA^{V5+}$ strains. Colony forming units (CFU) per organ were numerated at 48 h and 72 h post-infection in the spleens (A) and livers (B) of infected animals. Error bars indicate standard deviations. Statistically significant differences according to a two-tailed T-test were highlighted. *, $p < 0.05$; **, $p < 0.01$.

The colonization of organs by $\Delta IntA$ bacteria and by bacteria constitutively expressing *IntA-V5* from a multicopy plasmid was decreased compared to WT, both at 48 h (like in fig. 1B, right) and at 72 h post infection.

Supporting Tables

Table S1. Bacterial strains.

Name	Characteristics	Reference
BUG1600	<i>Listeria monocytogenes</i> EGDe	ATCC BAA-679 (1)
BUG2214	EGDe $\Delta prfA$	(40)
BUG2215	EGDe $\Delta sigB$	(40)
BUG2168	EGDe $\Delta lntA$	This work
BUG2169	EGDe $\Delta lntA$	This work
BUG2384	EGDe [pP1- <i>lntA-V5</i>] (referred to as <i>lntAv5+</i>)	This work
BUG2466	EGDe $\Delta lntA$ [pP1] (referred to as <i>lntA-</i>)	This work
BUG2820	EGDe $\Delta lntA$:pPL2 (referred to as <i>lntAc-</i>)	This work
BUG2822	EGDe $\Delta lntA$:pPL2- <i>P_{HYP}ER-5'-UTR_{hly}-lntA</i> (referred to as <i>lntAc+</i>)	This work

Table S2. Plasmids.

Name	Description	Tag (position)	Reference
pBUG942	pP1 multicopy plasmid with <i>P_{PRT}</i> promoter		(3)
pBUG2383	pP1- <i>lntA-V5</i>	V5 (C-ter)	This work
pBUG2387	pcDNA3.1/V5-His-TOPO- <i>lntA₃₄₋₂₀₅</i>	V5-His (C-ter)	This work
pBUG2388	pcDNA3.1/V5-His-TOPO- <i>mCFP</i>	V5-His (C-ter)	(6)
pBUG2389	pcDNA3.1/V5-His-TOPO- <i>BAHDI</i>	V5-His (C-ter)	(6)
pBUG2392	pE- <i>mCFP-N1-lntA₃₄₋₂₀₅</i>	mECFP (C-ter)	This work
pBUG2393	pB27- <i>lntA₃₄₋₂₀₅</i>	LexA (C-ter)	This work
pBUG2397	pET41a- <i>lntA₃₄₋₂₀₅</i>	GST-His (N-ter)	This work
pBUG2507	pMAD- $\Delta lntA$		This work
pBUG2809	pPL2- <i>P_{HYP}ER-5'-UTR_{hly}-lntA</i>		This work
pPL2	<i>Listeria monocytogenes</i> site-specific integration vector		(4)
pGEX- <i>lntA</i>	[pGEX-4T-1] <i>lntA₃₄₋₂₀₅</i>	GST (N-ter)	This work
pAG834	pcDNA5/FRT-HPT-blue	HPT (N-ter)	(5)
pAG978	pcDNA5/FRT/TO-HPT-blue	HPT (N-ter)	This work
pAG1190	pcDNA5/FRT/TO-HPT- <i>BAHDI</i>	HPT (N-ter)	This work

Table S3. Bacterial entry in LoVo cells is independent of *IntA* expression and is not altered by IFN- λ 2 treatment.**(A) Invasiveness of LoVo cells by *IntA*-expressing or non-expressing *L. monocytogenes*.**

The percentage of entry in epithelial cells for a MOI of 20 was quantified by a gentamicin survival assay. Results are expressed as percentage of the inoculum that survived the gentamicin test. Means \pm standard deviations (SD) were calculated on three biological replicates. This assay was reproduced independently at least three times and gave similar results. There was no significant difference between the strains in efficiency of entry.

	WT	$\Delta IntA$	<i>IntA</i>_{V5+}	<i>IntA</i>⁻	<i>IntA</i>_{c+}	<i>IntA</i>_{c-}
Inoculum (CFU/ml)	9.1 10 ⁶	9.7 10 ⁶	1.0 10 ⁷	9.3 10 ⁶	1.0 10 ⁷	9.5 10 ⁶
% entry (mean \pm SD)	0.78 \pm 0.12	0.80 \pm 0.06	0.85 \pm 0.01	0.92 \pm 0.05	0.93 \pm 0.19	0.99 \pm 0.19

(B) Invasiveness of IFN- λ -treated LoVo cells by *L. monocytogenes*.

Cells were incubated with increasing concentrations of IFN- λ 2 24h before being infected with WT bacteria. The level of entry for an inoculum of 5.10⁶ bacteria (MOI = 20) was quantified by a gentamicin survival assay. Results are expressed as above. This assay was reproduced twice and gave similar results. Pre-treatment of cells with IFN- λ 2 had no significant effect on bacterial entry into epithelial cells.

IFN-λ2 (ng/ml)	-	10	25	100	250
% entry (mean \pm SD)	0.81 \pm 0.07	0.89 \pm 0.16	0.87 \pm 0.24	0.92 \pm 0.05	0.83 \pm 0.29

Table S4. Transcriptome data – genes activated by LntA in infected LoVo cells.

The following table recapitulates the list of differentially modulated transcripts from Affymetrix Human Gene 1ST genechip data, in LoVo cells infected either with *lntA*^{V5+} or *lntA*⁻ strains. Only 324 up-regulated transcripts with a significantly different level in the comparison of samples after Benjamini Hochberg p-value adjustment ($p < 0,05$) and showing a minimum of 1.2 fold difference were considered. Complete data are available in the Gene Expression Omnibus Database (<http://www.ncbi.nlm.nih.gov/geo/>) with GEO accession number GSE26414. FC, Fold change (*lntA*^{V5+}/*lntA*⁻); p-value, adjusted p-value (Benjamini-Hochberg).

Genes belonging to the ISG regulon are highlighted as follows: green, interferon gene; yellow, annotated ISG from the interferome database (<http://www.interferome.org>); orange, annotated ISG from a manual bibliography search in the PubMed database (<http://www.ncbi.nlm.nih.gov/pubmed>); pink, predicted ISGs from the cisRED database (<http://www.cisred.org>). 39 genes with a fold change above 2 are highlighted in bold letterings.

Assignment	Gene name	Definition	FC	p-value
NM_003641	IFITM1	interferon induced transmembrane protein 1 (9-27)	4.03	0
NM_002053	GBP1	guanylate binding protein 1, interferon-inducible, 67kDa	3.63	0
NM_002535	OAS2	2-5-oligoadenylate synthetase 2, 69	3.53	0
NM_014070	C6orf15	chromosome 6 open reading frame 15	3.48	1.79E-12
NM_004585	RARRES3	retinoic acid receptor responder (tazarotene induced) 3	3.18	1.08E-11
NM_172138	IL28A	interleukin 28A (interferon, lambda 2)	3.14	0
NM_002463	MX2	myxovirus (influenza virus) resistance 2 (mouse)	3.05	0
NM_006820	IFI44L	interferon-induced protein 44-like	3.03	6.58E-10
NM_152703	SAMD9L	sterile alpha motif domain containing 9-like	2.99	1.92E-12
NM_017523	XAF1	XIAP associated factor-1	2.79	0
NM_172139	IL28B	interleukin 28B (interferon, lambda 3)	2.77	0
NM_004688	NMI	N-myc (and STAT) interactor	2.66	0
NM_080424	SP110	SP110 nuclear body protein	2.53	0
NM_004184	WARS	tryptophanyl-tRNA synthetase	2.51	0
NM_001565	CXCL10	chemokine (C-X-C motif) ligand 10	2.48	3.24E-05
NM_016582	SLC15A3	solute carrier family 15, member 3	2.48	0
NM_172140	IL29	interleukin 29 (interferon, lambda 1)	2.43	0
NM_006472	TXNIP	thioredoxin interacting protein	2.30	0
NM_003335	UBE1L	ubiquitin-activating enzyme E1-like	2.28	1.12E-05
NM_002985	CCL5	chemokine (C-C motif) ligand 5	2.27	5.36E-10
NM_001255	CDC20	cell division cycle 20 homolog (S. cerevisiae)	2.22	1.29E-12
NM_005516	HLA-E	major histocompatibility complex, class I, E	2.22	5.17E-06
NM_005030	PLK1	polo-like kinase 1 (Drosophila)	2.22	9.57E-12
NM_080657	RSAD2	radical S-adenosyl methionine domain containing 2	2.22	0
NM_005533	IFI35	interferon-induced protein 35	2.20	0
NM_003265	TLR3	toll-like receptor 3	2.20	7.75E-06
AJ583822	USP41	ubiquitin specific peptidase 41	2.19	0
NM_170672	RASGRP3	RAS guanyl releasing protein 3 (calcium and DAG-regulated)	2.17	5.29E-05
NM_001444	FABP5	fatty acid binding protein 5 (psoriasis-associated)	2.16	0
NM_005953	MT2A	metallothionein 2A	2.16	0
NM_001002264	EPSTI1	epithelial stromal interaction 1 (breast)	2.14	4.15E-07
NM_198433	AURKA	aurora kinase A	2.11	4.07E-06
NM_002800	PSMB9	proteasome (prosome, macropain) subunit, beta type, 9 (large multifunctional peptidase 2)	2.10	9.80E-12
NM_016816	OAS1	2,5-oligoadenylate synthetase 1, 40	2.07	0

Assignment	Gene name	Definition	FC	p-value
NM_145343	APOL1	apolipoprotein L, 1	2.06	3.92E-13
NM_018284	GBP3	guanylate binding protein 3	2.06	2.08E-04
NM_022147	RTP4	receptor (chemosensory) transporter protein 4	2.06	4.17E-05
NM_017414	USP18	ubiquitin specific peptidase 18	2.06	0
NM_001547	IFIT2	interferon-induced protein with tetratricopeptide repeats 2	2.01	3.55E-11
NM_014398	LAMP3	lysosomal-associated membrane protein 3	1.99	1.53E-11
NM_005733	KIF20A	kinesin family member 20A	1.97	1.49E-04
NM_001548	IFIT1	interferon-induced protein with tetratricopeptide repeats 1	1.96	0
NM_000798	DRD5	dopamine receptor D5	1.95	1.58E-04
NM_003141	TRIM21	tripartite motif-containing 21	1.95	1.51E-10
NM_006074	TRIM22	tripartite motif-containing 22	1.93	2.80E-02
NM_001031683	IFIT3	interferon-induced protein with tetratricopeptide repeats 3	1.92	2.02E-13
NM_002462	MX1	myxovirus (influenza virus) resistance 1, interferon-inducible protein p78 (mouse)	1.92	0
NM_003004	SECTM1	secreted and transmembrane 1	1.92	6.93E-09
NM_000526	KRT14	keratin 14 (epidermolysis bullosa simplex, Dowling-Meara, Koebner)	1.91	4.42E-10
NM_172208	TAPBP	TAP binding protein (tapasin)	1.91	1.35E-06
NM_006417	IFI44	interferon-induced protein 44	1.89	0
NM_004693	KRT75	keratin 75	1.89	3.81E-03
NM_006355	TRIM38	tripartite motif-containing 38	1.89	1.54E-08
NM_006479	RAD51AP1	RAD51 associated protein 1	1.88	1.37E-03
NM_018295	TMEM140	transmembrane protein 140	1.88	1.30E-03
NM_014750	DLG7	discs, large homolog 7 (Drosophila)	1.87	2.14E-04
NM_032545	CFC1	cripto, FRL-1, cryptic family 1	1.85	1.16E-02
NM_006877	GMPR	guanosine monophosphate reductase	1.85	1.42E-05
NM_020056	HLA-DQA2	major histocompatibility complex, class II, DQ alpha 2	1.85	0
NM_014831	LBA1	lupus brain antigen 1	1.84	8.76E-06
NM_005435	ARHGEF5	Rho guanine nucleotide exchange factor (GEF) 5	1.83	1.12E-05
NM_003521	HIST1H2BM	histone cluster 1, H2bm	1.83	2.11E-08
XR_017543	LOC400578	hypothetical gene supported by BC039169; NM_005557	1.83	7.48E-08
NM_031458	PARP9	poly (ADP-ribose) polymerase family, member 9	1.83	2.02E-13
NM_178517	PIGW	phosphatidylinositol glycan anchor biosynthesis, class W	1.83	6.31E-03
ENST00000298566	BCL2L14	BCL2-like 14 (apoptosis facilitator) (BCL2L14), transcript variant 3	1.82	7.96E-03
NM_031966	CCNB1	cyclin B1	1.82	1.24E-04
NM_000433	NCF2	neutrophil cytosolic factor 2	1.82	2.37E-06
NM_006994	BTN3A3	butyrophilin, subfamily 3, member A3	1.80	5.64E-03
NM_012420	IFIT5	interferon-induced protein with tetratricopeptide repeats 5	1.80	1.20E-07
NM_006101	NDC80	NDC80 homolog, kinetochore complex component (<i>S. cerevisiae</i>)	1.80	7.14E-03
NM_003733	OASL	2-5-oligoadenylate synthetase-like	1.80	9.85E-09
NM_022872	IFI6	interferon, alpha-inducible protein 6	1.78	0
NM_000625	NOS2A	nitric oxide synthase 2A (inducible, hepatocytes)	1.78	7.05E-04
NM_002983	CCL3	chemokine (C-C motif) ligand 3	1.77	7.31E-03
NM_017878	HRASLS2	HRAS-like suppressor 2	1.77	7.84E-03
NM_003561	PLA2G10	phospholipase A2, group X	1.77	2.12E-02
NM_004159	PSMB8	proteasome (prosome, macropain) subunit, beta type, 8 (large multifunctional peptidase 7)	1.77	1.30E-05
NM_000593	TAP1	transporter 1, ATP-binding cassette, sub-family B (MDR)	1.77	5.59E-10
NM_207315	LOC129607	hypothetical protein LOC129607	1.75	2.76E-08
NM_032206	NLRC5	NLR family, CARD domain containing 5	1.75	1.47E-04
NM_002129	HMGB2	high-mobility group box 2	1.74	1.58E-04
NM_006850	IL24	interleukin 24	1.74	6.91E-06
NM_000544	TAP2	transporter 2, ATP-binding cassette, sub-family B (MDR)	1.74	2.58E-05
NM_005557	KRT16	keratin 16 (focal non-epidermolytic palmoplantar keratoderma)	1.73	1.18E-03

Assignment	Gene name	Definition	FC	p-value
NM_022553	VPS52	vacuolar protein sorting 52 homolog (<i>S. cerevisiae</i>)	1.73	2.23E-06
NM_014783	ARHGAP11A	Rho GTPase activating protein 11A	1.72	4.64E-03
NM_138287	DTX3L	deltex 3-like (<i>Drosophila</i>)	1.72	3.59E-08
ENST00000326176	FLJ11286	hypothetical protein FLJ11286 (FLJ11286), mRNA	1.72	3.43E-07
NM_033109	PNPT1	polyribonucleotide nucleotidyltransferase 1	1.71	3.97E-11
NM_017654	SAMD9	sterile alpha motif domain containing 9	1.71	4.68E-08
NM_001237	CCNA2	cyclin A2	1.69	1.20E-04
NM_000422	KRT17	keratin 17	1.69	2.30E-04
NM_005419	STAT2	signal transducer and activator of transcription 2, 113kDa	1.69	1.04E-08
NM_181802	UBE2C	ubiquitin-conjugating enzyme E2C	1.69	1.25E-02
NM_021066	HIST1H2AJ	histone cluster 1, H2aj	1.68	2.27E-02
ENST00000369163	HIST2H3C	histone cluster 2, H3c (HIST2H3C), mRNA	1.68	8.41E-08
NM_004761	RGL2	ral guanine nucleotide dissociation stimulator-like 2	1.68	3.75E-02
NM_138456	BATF2	basic leucine zipper transcription factor, ATF-like 2	1.67	7.24E-04
NM_031299	CDCA3	cell division cycle associated 3	1.67	2.86E-03
NM_024119	DHX58	DEXH (Asp-Glu-X-His) box polypeptide 58	1.67	1.00E-05
NM_001098479	HLA-F	major histocompatibility complex, class I, F	1.67	2.24E-06
NM_021105	PLSCR1	phospholipid scramblase 1	1.67	1.88E-06
NM_001034841	LOC162073	hypothetical protein LOC162073	1.66	2.99E-05
NM_002818	PSME2	proteasome (prosome, macropain) activator subunit 2 (PA28 beta)	1.66	3.81E-05
NM_004223	UBE2L6	ubiquitin-conjugating enzyme E2L 6	1.66	1.40E-06
NM_031212	SLC25A28	solute carrier family 25, member 28	1.65	1.79E-03
NM_001786	CDC2	cell division cycle 2, G1 to S and G2 to M	1.64	4.99E-02
NM_014314	DDX58	DEAD (Asp-Glu-Ala-Asp) box polypeptide 58	1.64	1.24E-06
NM_018950	HLA-F	major histocompatibility complex, class I, F	1.64	4.03E-06
NM_007047	BTN3A2	butyrophilin, subfamily 3, member A2	1.62	1.45E-05
NM_014143	CD274	CD274 molecule	1.62	6.66E-04
NM_006435	IFITM2	interferon induced transmembrane protein 2 (1-8D)	1.62	1.85E-05
NM_002346	LY6E	lymphocyte antigen 6 complex, locus E	1.62	1.42E-05
NM_152649	MLKL	mixed lineage kinase domain-like	1.62	2.25E-03
NM_024956	TMEM62	transmembrane protein 62	1.62	6.56E-06
NM_016619	PLAC8	placenta-specific 8	1.61	6.42E-06
NM_001040458	ARTS-1	type 1 tumor necrosis factor receptor shedding aminopeptidase regulator	1.60	4.87E-02
NM_003529	HIST1H3A	histone cluster 1, H3a	1.60	1.67E-04
NM_003534	HIST1H3G	histone cluster 1, H3g	1.60	3.23E-02
NM_002166	ID2	inhibitor of DNA binding 2, dominant negative helix-loop-helix protein	1.60	3.39E-02
NM_005480	TROAP	trophinin associated protein (tastin)	1.60	4.21E-03
NM_017912	HERC6	hect domain and RLD 6	1.59	8.02E-05
NM_002659	PLAUR	plasminogen activator, urokinase receptor	1.59	9.29E-06
NM_001827	CKS2	CDC28 protein kinase regulatory subunit 2	1.58	2.18E-05
NM_004496	FOXA1	forkhead box A1	1.58	1.18E-03
NM_002214	ITGB8	integrin, beta 8	1.58	4.16E-02
NM_006342	TACC3	transforming, acidic coiled-coil containing protein 3	1.58	4.46E-02
NM_003246	THBS1	thrombospondin 1	1.58	3.89E-04
NM_052864	TIFA	TRAF-interacting protein with a forkhead-associated domain	1.58	1.95E-02
NM_003513	HIST1H2AB	histone cluster 1, H2ab	1.57	2.86E-03
NM_005516	HLA-E	major histocompatibility complex, class I, E	1.57	1.08E-06
NM_032844	MASTL	microtubule associated serine	1.57	2.31E-05
NM_005982	SIX1	SIX homeobox 1	1.57	1.59E-02
NM_198956	SP8	Sp8 transcription factor	1.57	1.24E-04
NM_006461	SPAG5	sperm associated antigen 5	1.57	2.78E-02
NM_004217	AURKB	aurora kinase B	1.56	4.63E-04

Assignment	Gene name	Definition	FC	p-value
NM_001251	CD68	CD68 molecule	1.56	2.49E-06
NM_002178	IGFBP6	insulin-like growth factor binding protein 6	1.56	2.73E-07
NM_005567	LGALS3BP	lectin, galactoside-binding, soluble, 3 binding protein	1.56	2.26E-06
NM_032789	PARP10	poly (ADP-ribose) polymerase family, member 10	1.56	1.30E-03
NM_001274	CHEK1	CHK1 checkpoint homolog (<i>S. pombe</i>)	1.55	1.74E-02
NM_001955	EDN1	endothelin 1	1.55	4.80E-02
NM_002116	HLA-A	major histocompatibility complex, class I, A	1.55	7.78E-07
NM_006845	KIF2C	kinesin family member 2C	1.55	6.44E-03
NM_002468	MYD88	myeloid differentiation primary response gene (88)	1.55	8.02E-05
NM_003981	PRC1	protein regulator of cytokinesis 1	1.55	6.24E-04
NM_001040874	HIST2H2AA4	histone cluster 2, H2aa4	1.54	2.55E-05
NM_003517	HIST2H2AC	histone cluster 2, H2ac	1.54	1.59E-06
NM_021059	HIST2H3C	histone cluster 2, H3c	1.54	1.49E-04
BC032140	HMG2	high-mobility group nucleosomal binding domain 2	1.54	6.99E-06
NM_021013	KRT34	keratin 34	1.54	4.37E-05
NM_004848	C1orf38	chromosome 1 open reading frame 38	1.53	8.02E-05
NM_152562	CDCA2	cell division cycle associated 2	1.53	2.16E-02
NM_012291	ESPL1	extra spindle pole bodies homolog 1 (<i>S. cerevisiae</i>)	1.53	5.04E-02
NM_202002	FOX1	forkhead box M1	1.53	4.00E-03
NM_002263	KIF1C	kinesin family member C1	1.53	1.96E-04
NM_033049	MUC13	mucin 13, cell surface associated	1.53	7.56E-05
NM_002485	NBN	nibrin	1.53	1.21E-02
NM_024515	WDR25	WD repeat domain 25	1.53	3.47E-02
NM_030641	APOL6	apolipoprotein L, 6	1.52	1.12E-02
NM_000775	CYP2J2	cytochrome P450, family 2, subfamily J, polypeptide 2	1.52	1.29E-02
ENST00000373451	KIAA0082	KIAA0082 (KIAA0082), mRNA	1.52	2.41E-04
NM_018438	FBX6	F-box protein 6	1.51	3.42E-03
AK131222	HSH2D	hematopoietic SH2 domain containing	1.51	4.99E-05
NM_000265	NCF1	neutrophil cytosolic factor 1	1.51	7.96E-03
NM_152905	NEDD1	neural precursor cell expressed, developmentally down-regulated 1	1.51	5.59E-04
NR_002961	SNORA22	small nucleolar RNA, H	1.51	6.63E-05
NM_002105	H2AFX	H2A histone family, member X	1.49	1.50E-03
NM_003528	HIST2H2BE	histone cluster 2, H2be	1.49	5.03E-03
NM_002116	HLA-A	major histocompatibility complex, class I, A	1.49	5.49E-03
NM_002201	ISG20	interferon stimulated exonuclease gene 20kDa	1.49	2.26E-03
NM_004776	B4GALT5	UDP-Gal:betaGlcNAc beta 1,4- galactosyltransferase, polypeptide 5	1.48	1.43E-04
NM_000235	LIPA	lipase A, lysosomal acid, cholesterol esterase (Wolman disease)	1.48	1.84E-03
NM_003827	NAPA	N-ethylmaleimide-sensitive factor attachment protein, alpha	1.48	8.53E-04
NM_001037335	PRIC285	peroxisomal proliferator-activated receptor A interacting complex 285	1.48	1.16E-03
uc002tfz.1	RGPD5	RANBP2-like and GRIP domain containing 5	1.48	3.36E-02
NM_018009	TAPBPL	TAP binding protein-like	1.48	2.10E-03
NM_020453	ATP10D	ATPase, Class V, type 10D	1.47	3.12E-02
BC126339	H2BFS	H2B histone family, member S	1.47	1.28E-03
NM_002117	HLA-C	major histocompatibility complex, class I, C	1.47	3.50E-04
NM_005532	IFI27	interferon, alpha-inducible protein 27	1.47	4.11E-04
NM_021034	IFITM3	interferon induced transmembrane protein 3 (1-8U)	1.47	9.13E-05
NM_005573	LMNB1	lamin B1	1.47	3.40E-03
AF193059	LOC26010	viral DNA polymerase-transactivated protein 6	1.47	1.83E-04
NM_016457	PRKD2	protein kinase D2	1.47	2.08E-04
ENST00000389055	PYROXD1	hypothetical protein FLJ22028 (FLJ22028), mRNA	1.47	4.64E-03
NM_007048	BTN3A1	butyrophilin, subfamily 3, member A1	1.46	2.06E-02
BC033660	DBF4B	DBF4 homolog B (<i>S. cerevisiae</i>)	1.46	3.55E-02

Assignment	Gene name	Definition	FC	p-value
NM_016095	GINS2	GINS complex subunit 2 (Psf2 homolog)	1.46	3.69E-02
NM_024736	GSDMDC1	gasdermin domain containing 1	1.46	1.30E-02
NM_006187	OAS3	2-5-oligoadenylate synthetase 3, 100kDa	1.46	2.39E-05
NM_017554	PARP14	poly (ADP-ribose) polymerase family, member 14	1.46	3.35E-05
NM_007315	STAT1	signal transducer and activator of transcription 1, 91kDa	1.46	4.05E-05
NM_203401	STMN1	stathmin 1	1.46	4.61E-02
ENST00000331615	TMEM106A	transmembrane protein 106A (TMEM106A), mRNA	1.46	2.40E-02
NM_005192	CDKN3	cyclin-dependent kinase inhibitor 3	1.45	3.20E-02
NM_001012967	FLJ31033	hypothetical protein FLJ31033	1.45	2.71E-03
AK023116	LOC93349	hypothetical protein BC004921	1.45	3.69E-02
NM_022346	NCAPG	non-SMC condensin I complex, subunit G	1.45	1.58E-04
NM_004346	CASP3	caspase 3, apoptosis-related cysteine peptidase	1.44	1.65E-02
NM_018101	CDCA8	cell division cycle associated 8	1.44	2.39E-02
NM_002006	FGF2	fibroblast growth factor 2 (basic)	1.44	5.86E-04
NM_003530	HIST1H3D	histone cluster 1, H3d	1.44	1.24E-03
NM_175065	HIST2H2AB	histone cluster 2, H2ab	1.44	1.59E-04
NM_005346	HSPA1B	heat shock 70kDa protein 1B	1.44	4.11E-04
NM_016359	NUSAP1	nucleolar and spindle associated protein 1	1.44	2.59E-03
NM_176783	PSME1	proteasome (prosome, macropain) activator subunit 1 (PA28 alpha)	1.44	1.62E-03
NM_031229	RBCK1	RanBP-type and C3HC4-type zinc finger containing 1	1.44	6.34E-03
NM_014501	UBE2S	ubiquitin-conjugating enzyme E2S	1.44	1.13E-02
NM_138441	C6orf150	chromosome 6 open reading frame 150	1.43	5.44E-03
NM_033133	CNP	2,3-cyclic nucleotide 3 phosphodiesterase	1.43	9.38E-03
NM_012100	DNPEP	aspartyl aminopeptidase	1.43	2.69E-03
AF087992	EIF5A	eukaryotic translation initiation factor 5A	1.43	1.56E-06
NM_003080	SMPD2	sphingomyelin phosphodiesterase 2, neutral membrane	1.43	8.12E-03
NR_002588	SNORA4	small nucleolar RNA, H	1.43	2.33E-02
NM_001001522	TAGLN	transgelin	1.43	7.14E-03
NM_004457	ACSL3	acyl-CoA synthetase long-chain family member 3	1.42	3.62E-02
NM_022168	IFIH1	interferon induced with helicase C domain 1	1.42	1.45E-04
NM_005101	ISG15	ISG15 ubiquitin-like modifier	1.42	1.79E-04
NM_020189	ENY2	enhancer of yellow 2 homolog (<i>Drosophila</i>)	1.41	3.39E-02
NM_001034194	EXOSC9	exosome component 9	1.41	1.80E-03
NM_033055	HIAT1	hippocampus abundant transcript 1	1.41	8.92E-03
NM_003537	HIST1H3B	histone cluster 1, H3b	1.41	2.19E-02
NM_173086	KRT6C	keratin 6C	1.41	3.78E-02
NM_031419	NFKBIZ	nuclear factor of kappa light polypeptide gene enhancer in B-cells inhibitor, zeta	1.41	2.05E-02
NM_007173	PRSS23	protease, serine, 23	1.41	3.40E-03
NM_004219	PTTG1	pituitary tumor-transforming 1	1.41	3.15E-02
ENST00000330794	TMEM173	transmembrane protein 173 (TMEM173), mRNA	1.41	1.91E-02
NM_001004196	CD200	CD200 molecule	1.40	2.48E-02
NM_004417	DUSP1	dual specificity phosphatase 1	1.40	5.84E-03
NM_030919	FAM83D	family with sequence similarity 83, member D	1.40	2.43E-02
NM_020238	INCENP	inner centromere protein antigens 135	1.40	4.43E-02
XM_929774	LOC646817	SET nuclear oncogene pseudogene	1.40	7.81E-03
NM_014321	ORC6L	origin recognition complex, subunit 6 like (yeast)	1.40	2.05E-02
NM_198490	RAB43	RAB43, member RAS oncogene family	1.40	1.04E-02
NM_144975	SLFN5	schlafen family member 5	1.40	8.41E-03
ENST00000263384	FAM32A	family with sequence similarity 32, member A (FAM32A), mRNA	1.39	4.43E-02
NM_001001555	GRB10	growth factor receptor-bound protein 10	1.39	1.06E-03
NM_003524	HIST1H2BH	histone cluster 1, H2bh	1.39	1.64E-02

Assignment	Gene name	Definition	FC	p-value
NM_006041	HS3ST3B1	heparan sulfate (glucosamine) 3-O-sulfotransferase 3B1	1.39	4.61E-02
NM_006332	IFI30	interferon, gamma-inducible protein 30	1.39	2.05E-02
NM_002198	IRF1	interferon regulatory factor 1	1.39	1.02E-02
NM_015907	LAP3	leucine aminopeptidase 3	1.39	3.55E-02
NM_021127	PMAIP1	phorbol-12-myristate-13-acetate-induced protein 1	1.39	3.78E-03
ENST00000305363	TMPRSS11E	transmembrane protease, serine 11E (TMPRSS11E), mRNA	1.39	3.31E-03
NM_001079539	XBP1	X-box binding protein 1	1.39	2.57E-03
NM_030882	APOL2	apolipoprotein L, 2	1.39	2.31E-05
NM_212482	FN1	fibronectin 1	1.39	4.41E-02
NM_005322	HIST1H1B	histone cluster 1, H1b	1.39	1.49E-04
NM_002451	MTAP	methylthioadenosine phosphorylase	1.39	2.86E-03
NR_002754	RNU5E	RNA, U5E small nuclear	1.39	1.50E-03
NM_025075	THOC7	THO complex 7 homolog (<i>Drosophila</i>)	1.39	1.17E-02
NM_020119	ZC3HAV1	zinc finger CCCH-type, antiviral 1	1.39	7.44E-04
NM_022488	ATG3	ATG3 autophagy related 3 homolog (<i>S. cerevisiae</i>)	1.38	1.70E-02
NM_174983	C19orf28	chromosome 19 open reading frame 28	1.38	3.85E-02
NM_002388	MCM3	minichromosome maintenance complex component 3	1.38	4.42E-02
NM_022061	MRPL17	mitochondrial ribosomal protein L17	1.38	2.73E-02
ENST00000314842	RPL41	ribosomal protein L41 (RPL41), transcript variant 2, mRNA	1.38	2.68E-02
NM_033518	SLC38A5	solute carrier family 38, member 5	1.38	3.14E-02
NM_001080391	SP100	SP100 nuclear antigen	1.38	9.88E-03
NM_007109	TCF19	transcription factor 19 (SC1)	1.38	4.45E-04
NM_014290	TDRD7	tudor domain containing 7	1.38	3.85E-02
NM_033034	TRIM5	tripartite motif-containing 5	1.38	6.67E-03
NM_033286	C15orf23	chromosome 15 open reading frame 23	1.37	4.99E-02
NM_012193	FZD4	frizzled homolog 4 (<i>Drosophila</i>)	1.37	2.90E-02
NM_022750	PARP12	poly (ADP-ribose) polymerase family, member 12	1.37	3.82E-03
NM_006915	RP2	retinitis pigmentosa 2 (X-linked recessive)	1.37	4.99E-02
NM_003132	SRM	spermidine synthase	1.37	7.93E-03
NM_012342	BAMBI	BMP and activin membrane-bound inhibitor homolog (<i>Xenopus laevis</i>)	1.36	2.42E-02
NM_021018	HIST1H3F	histone cluster 1, H3f	1.36	1.13E-02
NM_005514	HLA-B	major histocompatibility complex, class I, B	1.36	2.48E-04
NM_002357	MXD1	MAX dimerization protein 1	1.36	1.12E-02
NM_013290	PSMC3IP	PSMC3 interacting protein	1.36	3.96E-02
NM_001007230	SPOP	speckle-type POZ protein	1.36	7.14E-03
NM_024092	TMEM109	transmembrane protein 109	1.36	5.19E-03
NM_003541	HIST1H4K	histone cluster 1, H4k	1.35	1.17E-02
BC020891	HLA-G	HLA-G histocompatibility antigen, class I, G	1.35	1.03E-02
NM_020529	NFKBIA	nuclear factor of kappa light polypeptide gene enhancer in B-cells inhibitor, alpha	1.35	4.39E-03
NM_001657	AREG	amphiregulin (schwannoma-derived growth factor)	1.34	3.54E-02
NM_015161	ARL6IP1	ADP-ribosylation factor-like 6 interacting protein 1	1.34	5.40E-03
NM_016289	CAB39	calcium binding protein 39	1.34	4.36E-03
NM_001826	CKS1B	CDC28 protein kinase regulatory subunit 1B	1.34	3.69E-02
NM_015634	KIAA1279	KIAA1279	1.34	1.18E-02
NM_006739	MCM5	minichromosome maintenance complex component 5	1.34	2.36E-02
NM_003542	HIST1H4C	histone cluster 1, H4c	1.33	1.14E-02
NM_002228	JUN	jun oncogene	1.33	3.14E-03
XR_015269	HIST2H2BE	histone cluster 2, H2be	1.33	2.82E-02
NM_015474	SAMHD1	SAM domain and HD domain 1	1.33	4.56E-02
NM_001307	CLDN7	claudin 7	1.32	4.49E-02
NM_172373	ELF1	E74-like factor 1 (ets domain transcription factor)	1.32	4.47E-02

Assignment	Gene name	Definition	FC	p-value
NM_018088	FAM90A1	family with sequence similarity 90, member A1	1.32	1.17E-02
NM_020150	SAR1A	SAR1 gene homolog A (<i>S. cerevisiae</i>)	1.32	3.39E-02
NM_024546	C13orf7	chromosome 13 open reading frame 7	1.31	4.43E-02
NM_020409	MRPL47	mitochondrial ribosomal protein L47	1.31	7.06E-03
NM_007346	OGFR	opioid growth factor receptor	1.31	4.86E-03
NM_003190	TAPBP	TAP binding protein (tapasin)	1.31	1.29E-02
NM_006088	TUBB2C	tubulin, beta 2C	1.31	3.47E-02
NM_001085411	C5orf33	chromosome 5 open reading frame 33	1.30	1.86E-02
XM_001132216	LOC644589	similar to translocase of the inner mitochondrial membrane 14 isoform a	1.30	9.48E-04
NM_052886	MAL2	mal, T-cell differentiation protein 2	1.30	1.04E-02
NM_020963	MOV10	Mov10, Moloney leukemia virus 10, homolog (mouse)	1.30	3.69E-02
NM_004289	NFE2L3	nuclear factor (erythroid-derived 2)-like 3	1.30	1.63E-02
NM_002823	PTMA	prothymosin, alpha (gene sequence 28)	1.30	6.96E-03
NM_182965	SPHK1	sphingosine kinase 1	1.30	3.20E-02
NM_004335	BST2	bone marrow stromal cell antigen 2	1.29	1.70E-02
NM_002467	MYC	v-myc myelocytomatosis viral oncogene homolog (avian)	1.29	2.52E-02
NM_001042616	PIGY	phosphatidylinositol glycan anchor biosynthesis, class Y	1.29	4.66E-02
NM_130900	RAET1L	retinoic acid early transcript 1L	1.29	2.80E-02
NM_000043	FAS	Fas (TNF receptor superfamily, member 6)	1.28	4.29E-02
NM_005324	H3F3B	H3 histone, family 3B (H3.3B)	1.28	4.45E-02
NM_003533	HIST1H3I	histone cluster 1, H3i	1.28	7.78E-03
NM_001012333	MDK	midkine (neurite growth-promoting factor 2)	1.27	4.96E-02
NM_002759	EIF2AK2	eukaryotic translation initiation factor 2-alpha kinase 2	1.27	2.10E-02
NM_005321	HIST1H1E	histone cluster 1, H1e	1.27	1.25E-02
NR_002564	SNORD26	small nucleolar RNA, C	1.26	1.03E-02
NR_002559	SNORD29	small nucleolar RNA, C	1.26	2.02E-02
NM_004640	BAT1	HLA-B associated transcript 1	1.25	2.16E-02
NM_007317	KIF22	kinesin family member 22	1.24	2.30E-06
ENST00000336176	TMEM106B	transmembrane protein 106B (TMEM106B), mRNA	1.23	2.43E-02
NM_001083538	POTE2	protein expressed in prostate, ovary, testis, and placenta 2	1.22	4.63E-02
NM_002116	HLA-A	major histocompatibility complex, class I, A	1.21	3.61E-02
XR_018749	KRT18	keratin 18	1.21	1.08E-02
NM_032026	TATDN1	TatD DNase domain containing 1	1.21	1.06E-04

Table S5. Oligonucleotides.

Cloning			
Name	(RS)-Gene	Sequence	Reference
438-S1	(<i>Bam</i> HI)-5' <i>lntA</i>	CGCGGATCCGGAATCGCGCACACTTTC	This work
438-S2	(<i>Stu</i> I)-5' <i>lntA</i>	AAAAGGCCTTCTTCACTCGTTTTCTTC	This work
438-S3	(<i>Stu</i> I)-3' <i>lntA</i>	AAAAGGCCTAAGAAAAAGCCGTCTACAGA	This work
438-S4	(<i>Eco</i> RI)-3' <i>lntA</i>	CCGGAATTCTATGCAAAAAGACGATGCG	This work
oHB1	(<i>Eco</i> RI)- <i>lntA</i>	CGGAATTCATGGGAGAGGATGAAGGTGAAC	This work
oHB2	(<i>Xho</i> I)- <i>lntA</i>	CCGCTCGAGTTTTTTGACTATCCAATAATTC	This work
oHB3	(<i>Sac</i> I)- <i>lntA</i>	ACGAGCTCTGAAAGAAGGGAAAACGAGTG	This work
oHB4	<i>lntA</i>	AGTAACCATCGATTTGCTG	This work
oHB5	(<i>Sph</i> I)- <i>V5</i>	ACATGCATGCTTAACCGGTACGCGTAGAATC	This work
oDB1	(<i>Eag</i> I)-5' <i>hly</i>	GAGTCACGGCCGATAAAGCAAGCATATAATA	(41)
oDB2	5' <i>hly</i>	GGGTTTCACTCTCCTTCTACA	(41)
oAL17	5' <i>hly-lntA</i>	GTTAAAAAATGTAGAAGGAGAGTGAAACCCATG aagaagttagttgcttggtt	This work
oAL18	(<i>Sal</i> I)- <i>lntA</i>	GTCGACTTACTGCAGTTTTTTGACTATCCAATAATTCGTA	This work
oVJ1	(<i>Bam</i> HI)- <i>lntA</i>	AAAGGATCCATGGGAGAGGATGAAGGTGAAC	This work
oVJ2	(<i>Xho</i> I)- <i>lntA</i>	TCCCTCGAGTCATTTTTGACTATCCAATAATTCGTAGCC	This work
oGL1	(<i>Fse</i> I)- <i>BAHD1</i>	ATGCGGCCCGCCCATGACACACACTCGGAGAAAAG	This work
oGL2	(<i>Asc</i> I)- <i>BAHD1</i>	AGGCGCGCCCTACTGGGGTTCTTAAGGA	This work
qRT-PCR on cDNA			
Name	Gene	Sequence	Reference
gyrA-RT1	<i>gyrA</i>	GCGATGAGTGTAATTGTTG	(39)
gyrA-RT2	<i>gyrA</i>	ATCAGAAGTCATACCTAAGTC	(39)
hly-RT1	<i>hly</i>	GCTTGAATGTAAACTTCGG	This work
hly-RT2	<i>hly</i>	GCAACTGCTCTTTAGTAAC	This work
inlA-RT1	<i>inlA</i>	ACACGGTCTCACAAAACAG	(39)
inlA-RT2	<i>inlA</i>	TCAAGTATTCCTCCATCG	(39)
438-RT1	<i>lntA</i>	GGAGAGGATGAAGGTGAAC	This work
438-RT2	<i>lntA</i>	TCAAGGCTAAATCTTTGGTTG	This work
16S-RT1	<i>16S rRNA</i>	CTCGTGTCGTGAGATGTTGG	(20)
16S-RT2	<i>16S rRNA</i>	CGTGTGTAGCCCAGGTCATA	(20)
2845-RT1	<i>lmo2845</i>	GGTGTAGGAAGTCCATCGGACC	(20)
2845-RT2	<i>lmo2845</i>	ACTGCGCGCCAACCATTTGTAGC	(20)
qRT-PCR on ChIP samples			
Name	Gene	Sequence	Reference
IGF2-P3-b-F	<i>IGF2</i>	AAATTTGGGCATTGTTCCCGGCTC	(6)
IGF2-P3-b-R	<i>IGF2</i>	TGTGTTTGGGCAACGCTAGAGAGA	(6)
CD44-CpG-F	<i>CD44</i>	TATTTACAGCCTCAGCAGAGCACG	(6)

CD44-CpG-R	<i>CD44</i>	AAACAGTGACCTAAGACGGAGGGA	(6)
IFIT3-TS-F	<i>IFIT3</i>	AAAGCACAGACCTAACAGCACCCCT	(30)
IFIT3-TS-R	<i>IFIT3</i>	CATGATGGCTGTTTCCCTGCAGTT	(30)
IFITM1-e1-R	<i>IFITM1</i>	AAGGTCCACCGTGATCAACATCCA	This work
IFITM1-e1-F	<i>IFITM1</i>	AGTAGGCGAATGCTATGAAGCCCA	This work

BAHD1 KO mice – PCR validation of ES clones

Name	PCR product	Sequence	Reference
Ef1	5' external	TTATAGGCGCGCCAGAAATTGACAAAAGTCAGACCTGG	This work
Nr1	(4.9 kb)	GCGGCCGAGAACCTGCGTGCAATC	This work

BAHD1 KO mice – external-probe synthesis

Name	Sequence	Reference
probe2-F	GGTCTTACGTCCAGTGTTTCAGGACC	This work
probe2-R	CGCCAACCTCCCATGTCTGTTAGAGA	This work

BAHD1 KO mice – Genotyping

Name	Position	Sequence	Reference
4582	Ef	TACCCTGCAGGCAGGTTCTCCG	This work
5488	Ef	GCAGCACTCCTCAGACTGGCAGG	This work
4583	Er	TGGCCAAGCTAGTGCTGGCAACC	This work
4584	Er	CCCACACCACAAACGGAGTGCC	This work
255	Nf	AATGCCTGCTCTTTACTGAAGGCTC	This work
4587	Lxr	GAAGTTATACTAGAGCGGCC	This work
548	Nr	CCAGACTGCCTTGGGAAAAG	This work
4585	Wf	GTGTGTGTCGATCCTGGTTTCC	This work
4586	Wr	AGTGTGTGTCATGGAATCCCTC	This work

Table S6. PCR products and digests for the validation of BAHD1^{+/-} mice.**(A) Digestions used to validate the 5' and 3' insertion**

Four different digests were used to validate correct homologous recombination events. Two digests validate the 5' insertion, 3 other digests validate the 3' insertion.

Probe	Digest	Enzyme	WT allele (kb)	Targeted Allele (kb)
Neo (probe1)	5'-first	<i>Afl</i> III	—	11.8
	5'-second	<i>Eco</i> RV	—	8.9
	3'-first	<i>Acc</i> I	—	7.5
	3'-second	<i>B</i> lpI	—	9.2
	3'-third	<i>B</i> stBI	—	21.4

(B) Digestions used to validate with external probe

Probe	Digest	Enzyme	WT allele (kb)	Targeted Allele (kb)
5' external (probe2)	first	<i>A</i> paI	15.5	11.6
	second	<i>H</i> paI	15.5	8.5
	third	<i>E</i> coRI	6.8	11.0

(C) PCR fragments for genotyping (expected size in bp)

Region analyzed	Primers	Position (fig. S10)	WT allele	Targeted allele (L2)	KO allele (L-)
WT allele specific PCR (5' part of the targeted locus)	4582-4586	Ef / Wr	497	†	†
WT allele specific PCR (3' part of the targeted locus)	4585-4583	Wf / Er	433	†	†
5' part of the Neo marker	4582-548	Ef / Nr	†	499	†
3' part of the Neo marker	255-4583	Nf / Er	†	453	†
Excision of the Neo marker	4582-4584	Ef / Er	9515*	2520*	851
LoxP specific PCR	4582-4587	Ef / Lxr	†	423	423

* This PCR product was not observed using our PCR genotyping conditions.

† No Amplicon should be obtained.

Table S7. Crystallography. Data collection, phasing and refinement statistics.

LntA structure data are deposited at the Worldwide Protein Data Bank (<http://www ww p d b . o r g />), ID #2x14, structure factor file #r2x14sf.

Data collection	
Data set	Se Met Peak
Wavelength (Å)	0.979
Space group	P41212
a (Å)	49.7
b (Å)	49.7
c (Å)	141.8
Resolution (Å) (last shell limits)	2.3 (2.4-2.3)
No. observed/unique reflections	223,287/14,639
Completeness (%)	96.7 (91.4)
Rmeas (last shell)	8.4 (51.8)
Rmrgd-F (last shell)	5.4 (23.2)
I/σ(I) (last shell)	27.45 (8.3)
Phasing	
Phasing power ano	2.620
FOMobs	0.1062
FOMDM	0.5063
Refinement	
Resolution (Å)	2.3
Rwork (%)	23.22
Rfree (%)	25.52
No. of protein atoms	1,210
No. of solvent atoms	41
RMS deviation, bond lengths (Å)	0.02
RMS deviation, bond angles (°)	1.972
Mean B factor (Å ²)	39.26
Residues in most favored/allowed/outlier region of Ramachandran plot (total)	136/6/0 (142)

References

1. P. Glaser *et al.*, *Science* **294**, 849 (Oct 26, 2001).
2. A. Miyawaki, R. Y. Tsien, *Meth Enzymol* **327**, 472 (Jan 1, 2000).
3. S. Dramsi *et al.*, *Mol Microbiol* **16**, 251 (Apr 1, 1995).
4. P. Lauer, M. Y. N. Chow, M. J. Loessner, D. A. Portnoy, R. Calendar, *J Bacteriol* **184**, 4177 (Aug 1, 2002).
5. E. Derivery *et al.*, *Dev Cell* **17**, 712 (Nov, 2009).
6. H. Bierne *et al.*, *Proc Natl Acad Sci U S A* **106**, 13826 (Aug 18, 2009).
7. E. Derivery, A. Gautreau, *Methods Enzymol* **484**, 677 (2010).
8. E. Gouin *et al.*, *Proc Natl Acad Sci U S A* **107**, 17333 (Oct 5, 2010).
9. P. Steffen *et al.*, *Cell Motil Cytoskeleton* **45**, 58 (Jan 1, 2000).
10. D. Ribet *et al.*, *Nature* **464**, 1192 (Apr 22, 2010).
11. H. M. Cooper, Y. Paterson, *Curr Protoc Immunol* **Chapter 2**, Unit 2.4 (May 1, 2001).
12. M. Fromont-Racine, J. C. Rain, P. Legrain, *Nat Genet* **16**, 277 (Jul 1, 1997).
13. E. Formstecher *et al.*, *Genome Res* **15**, 376 (Mar 1, 2005).
14. S. F. Altschul *et al.*, *Nucleic Acids Res* **25**, 3389 (Sep 1, 1997).
15. H. Bierne *et al.*, *J Cell Sci* **118**, 1537 (Apr 1, 2005).
16. J. Pizarro-Cerda, M. Lecuit, P. Cossart, in *Molecular Cellular Microbiology*. (Academic Press Inc, San Diego, 2002), vol. 31, pp. 161-177.
17. R. Jonquières, H. Bierne, F. Fiedler, P. Gounon, P. Cossart, *Mol Microbiol* **34**, 902 (Dec 1, 1999).
18. H. Boukarabila *et al.*, *Genes Dev* **23**, 1195 (May 15, 2009).
19. C. Cheers, I. F. McKenzie, *Infect Immun* **19**, 755 (Mar, 1978).
20. A. Camejo *et al.*, *PLoS Pathog* **5**, e1000449 (May 1, 2009).
21. U. K. Laemmli, *Nature* **227**, 680 (Aug 15, 1970).
22. W. Kabsch, *Acta Crystallogr D Biol Crystallogr* **66**, 125 (Feb 1, 2010).
23. G. Bricogne, C. Vornrhein, C. Flensburg, M. Schiltz, W. Paciorek, *Acta Crystallogr D Biol Crystallogr* **59**, 2023 (Nov 1, 2003).
24. E. de La Fortelle, G. Bricogne, Charles W. Carter, Jr., in *Methods in Enzymology*. (Academic Press, 1997), vol. Volume 276, pp. 472-494.
25. P. Emsley, K. Cowtan, *Acta Crystallogr D Biol Crystallogr* **60**, 2126 (Dec 1, 2004).
26. A. Perrakis, R. Morris, V. S. Lamzin, *Nat Struct Biol* **6**, 458 (May 1, 1999).
27. G. N. Murshudov, A. A. Vagin, E. J. Dodson, *Acta Crystallogr D Biol Crystallogr* **53**, 240 (May 1, 1997).
28. L. Fritsch *et al.*, *Mol Cell* **37**, 46 (Jan 15, 2010).
29. C. Sabet, M. Lecuit, D. Cabanes, P. Cossart, H. Bierne, *Infect Immun* **73**, 6912 (Oct 1, 2005).
30. M. Lavigne *et al.*, *PLoS Genet* **5**, e1000769 (Dec, 2009).
31. S. Stockinger, T. Decker, *Immunobiology* **213**, 889 (2008).
32. L. A. Zenewicz, H. Shen, *Microbes Infect* **9**, 1208 (Aug, 2007).
33. C. Sommereyns, S. Paul, P. Staeheli, T. Michiels, *PLoS Pathog* **4**, e1000017 (Mar, 2008).
34. M. Mordstein *et al.*, *J Virol* **84**, 5670 (Jun, 2010).
35. M. Trost *et al.*, *Proteomics* **5**, 1544 (Apr, 2005).
36. H. Bierne, P. Cossart, *Microbiol Mol Biol Rev* **71**, 377 (Jun, 2007).
37. N. E. Freitag, G. C. Port, M. D. Miner, *Nat Rev Microbiol* **7**, 623 (Sep, 2009).
38. R. D. Sleator, D. Watson, C. Hill, C. G. Gahan, *Microbiology* **155**, 2463 (Aug, 2009).
39. C. Sabet *et al.*, *Infect Immun* **76**, 1368 (Apr, 2008).

40. P. Mandin, F. Repoila, M. Vergassola, T. Geissmann, P. Cossart, *Nucleic Acids Res* **35**, 962 (Jan 1, 2007).
41. D. Balestrino *et al.*, *Appl Environ Microbiol*, (Apr 2, 2010).